The roles of phylogeny, body size and substrate use in trabecular bone variation among Philippine 'earthworm mice' (Rodentia: Chrotomyini)

STEPHANIE M. SMITH^{1*,o}, DAKOTA M. ROWSEY², JONATHAN A. NATIONS^{1,3}, KENNETH D. ANGIELCZYK¹ and LAWRENCE R. HEANEY¹

Received 12 January 2023; revised 28 February 2023; accepted for publication 15 March 2023

Trabecular bone is modelled throughout an animal's life in response to its mechanical environment, but like other skeletal anatomy, it is also subject to evolutionary influences. Yet the relative strengths of factors that affect trabecular bone architecture are little studied. We investigated these influences across the Philippine endemic murine rodent clade Chrotomyini. These mammals have robustly established phylogenetic relationships, exhibit a range of well-documented substrate-use types, and have a body size range spanning several hundred grammes, making them ideal for a tractable study of extrinsic and intrinsic influences on trabecular bone morphology. We found slight differences in vertebral trabecular bone among different substrate-use categories, with more divergent characteristics in more ecologically specialized taxa. This suggests that the mechanical environment must be relatively extreme to affect trabecular bone morphology in small mammals. We also recovered allometric patterns that imply that selective pressures on bone may differ between small and large mammals. Finally, we found high intrataxonomic variation in trabecular bone morphology, but it is not clearly related to any variable we measured, and may represent a normal degree of variation in these animals rather than a functional trait. Future studies should address how this plasticity affects biomechanical properties and performance of the skeleton.

 $ADDITIONAL\ KEYWORDS:\ allometry-biomechanics-functional\ morphology-locomotor\ mode-Muridae, plasticity-substrate\ use-trabecular\ bone-vertebrae.$

INTRODUCTION

Trabecular bone, also called cancellous or spongy bone, is a bone tissue that forms a supportive scaffolding inside vertebrae, limb bones and cranial bones of vertebrates. This type of tissue plays an important role in the way vertebrate animals withstand everyday physical forces in their environments (Keaveny & Hayes, 1993; Smit *et al.*, 1997). The concept of bone functional adaptation (Wolff, 1893; Lanyon *et al.*, 1982; Cowin, 1986; Ruff *et al.*, 2006; Kivell, 2016) states that both trabecular and cortical bone morphology changes throughout an animal's lifetime in order to better withstand typical forces that act on the skeleton, but

¹Negaunee Integrative Research Center, Field Museum of Natural History, 1400 South DuSable Lake Shore Drive, Chicago, IL 60605, USA

²School of Life Sciences, Arizona State University, 734 West Alameda Drive, Tempe, AZ 85282, USA ³Department of the Geophysical Sciences, University of Chicago, 5734 South Ellis Avenue, Chicago, IL 60637, USA

trabecular bone models more quickly (Huiskes et al., 2000; Currey, 2003) and can yield a snapshot of a bone's mechanical environment. Artificial manipulation of a bone's mechanical environment, such as through compressive loading (Main et al., 2020), can yield a variety of changes in trabecular bone architecture, including changes in trabecular bone volume fraction and trabecular thickness (Main et al., 2014; Poulet et al., 2015), as well as trabecular orientation (Barak et al., 2011). Yet, like other aspects of morphology (Seilacher, 1970; Briggs, 2017), trabecular bone structure is influenced by a number of factors. Body size (Doube et al., 2011; Barak et al., 2013; Fajardo et al., 2013; Ryan & Shaw, 2013; Christen et al., 2015; Wysocki & Tseng, 2018; Saers et al., 2019; Webb, 2021), phylogenetic relationships (Ryan & Shaw, 2013; Plasse

^{*}Corresponding author. E-mail: smsmith@fieldmuseum.org

et al., 2019; Webb, 2021; Zack et al., 2022), ecology (Ryan & Shaw, 2012; Rolvien et al., 2017; Mielke et al., 2018; Dunmore et al., 2019; Amson & Bibi, 2021) and ontogeny (Tanck et al., 2001; Ryan & Krovitz, 2006; Gorissen et al., 2016) all may explain portions of the variation in trabecular bone morphology of wild mammal populations.

The degree to which each of these intrinsic and extrinsic factors influences trabecular bone morphology varies by clade and anatomical location, and different types of trabecular measurements correlate with different aspects of the scale and ecology of an organism. For example, in mammals, many studies find a strong correlation between trabecular thickness and body mass (e.g., Doube et al., 2011; Barak et al., 2013; Amson & Bibi, 2021), but the scaling of trabecular thickness may be negatively allometric or isometric depending on the body size range of animals included, and whether the tissue studied is sourced from the vertebral column, femur or humerus (Swartz et al., 1998; Doube et al., 2011; Ryan & Shaw, 2013; Mielke et al., 2018; Amson & Bibi, 2021). Bone volume fraction, or the proportion of bone relative to non-bone material in a given sample, has been found to be independent of body mass when examining the femoral head across a large range of body masses (Doube et al., 2011), but shows positive allometry in the femora of a smallerbodied mammal clade (Mielke et al., 2018), and in vertebrae across a diverse sample with a larger bodysize range (Amson & Bibi, 2021).

Locomotor ecology also appears to affect trabecular bone differently depending on clade, body size range and anatomical location examined. 'Lifestyle' (suspensory, arboreal or terrestrial) can be distinguished in xenarthrans using trabecular anisotropy of the forelimb, but digging style cannot be resolved (Amson et al., 2017). In sciurids, a variety of trabecular bone metrics correlate with locomotor mode (Mielke et al., 2018). In other mammalian groups, only highly specialized locomotor modes (e.g., saltatory/ricochetal, vertical clinging and leaping) differ markedly in trabecular bone structure (Fajardo et al., 2007a; Webb, 2021). Sometimes phylogenetic context implies that trabecular differences among locomotor modes are spurious (Webb, 2021); in other cases, results indicate very little phylogenetic influence on trabecular bone characteristics (Amson & Bibi, 2021).

Given the complexity of our current state of knowledge regarding trabecular bone in wild animal groups, we chose to execute a highly focused study to elucidate the influences on trabecular bone structure in small mammals specifically. To understand the biology of mammalian trabecular bone, it is imperative to understand the factors that influence its morphology in small-bodied species, because, according to one database, 83% of mammalian species weigh 5 kg or

less (Jones et al., 2009). Relatively few trabecular bone studies focus on this end of the mammalian body size spectrum in wild mammals (Mielke et al., 2018), but knowing how trabecular bone is shaped in small mammals could also lend powerful tools to workers interested in using museum specimens to document the ecologies of rare, endangered and/or difficult to catch small mammals with cryptic ecologies (Smith & Angielczyk, 2020). Furthermore, although many studies sample multiple specimens of a single species to capture intraspecific variation in trabecular bone traits (e.g., Webb, 2021), these results are not often discussed on their own, with the focus more often falling on body size or locomotor correlations. This poses a problem for workers using trabecular bone for functional morphology or ecomorphology: if we have no sense of 'normal' variation for a trait, how can we determine what is functionally important or 'unusual'?

For this study, we chose to examine the endemic Philippine radiation of murine rodents commonly referred to as 'earthworm mice' (Heaney et al., 2016a). Members of this clade (Chrotomyini sensu Rowsey et al., 2018) represent an adaptive ecological and morphological radiation, with five genera and approximately 45 species ranging from 23-225 g in mass (Heaney et al., 2016a) (Fig. 1). Morphologically, these rodents range from small shrew-like animals to larger, more typical, terrestrial rat-shaped animals, to robust subterranean foragers, to longsnouted earthworm specialists that move using a combination of walking and bounding (Heaney et al., 2016a). Extensive field studies have produced large series of museum-preserved whole-body and skeletal specimens, and intensive study of phylogenetic relationships, morphology, species richness, ecology and biogeography of these species has provided an evolutionary framework and a wealth of associated data (e.g., Jansa et al., 2006; Justiniano et al., 2015; Heanev et al., 2016a, b: Rowsev et al., 2018, 2019, 2020: Petrosky et al., 2021). This multifaceted scientific framework and detailed specimen record make the Chrotomyini an excellent test case for investigating the interplay of influences on trabecular bone morphology. Additionally, this system is unusual among those typically used in trabecular bone studies because all of the animals in our sample occur sympatrically, and have spent their entire history (approximately 8 Myr; Rowsey et al., 2018) evolving in close proximity to one another (Heaney et al., 2016a). In this way, the chrotomyin radiation represents a kind of natural controlled experiment. Variables like climate are largely controlled for (notwithstanding some variation due to elevation), but the variation in the clade allows us to consider how the evolution of trabecular bone features might be influenced by resource partitioning within the broader mammalian assemblage.

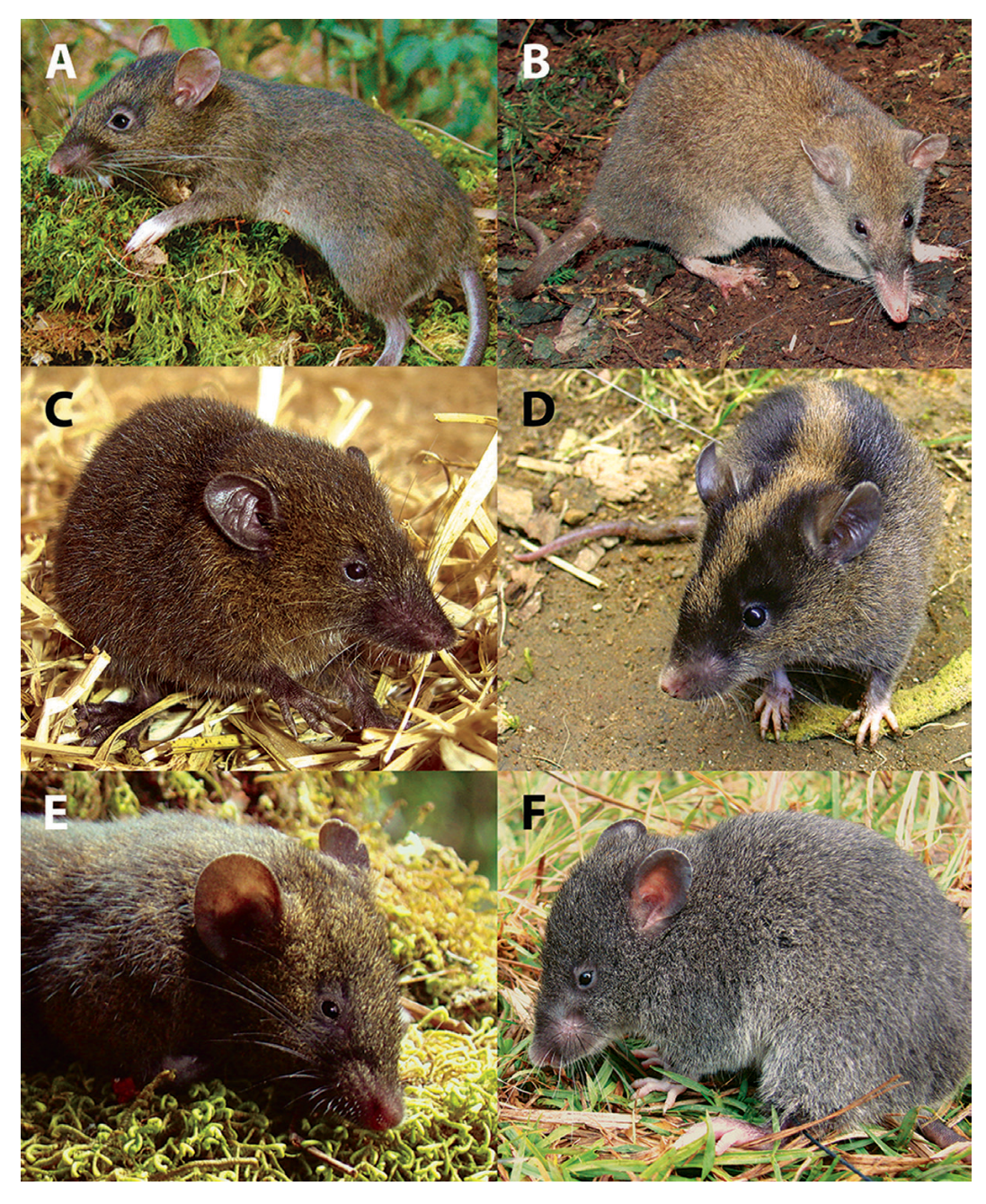


Figure 1. Photographic examples of chrotomyin genera and species included in this study. Body masses from Heaney *et al.* (2016a) are included here for a sense of animal size. A, *Apomys datae*, mass = 67–105 g. B, *Rhynchomys soricoides*, 133–225 g. Note: this species of *Rhynchomys* was not included here, but we had no images of our included species, *R. labo* (134–182 g). This image is intended to demonstrate the general morphology of the genus, in particular the elongate skull. C, *Soricomys montanus*, 23–31 g. D, *Chrotomys whiteheadi*, 105–190 g. E, *Archboldomys maximus*, 40–55 g. F, *Chrotomys silaceus*, 71–160 g. A, photograph by LR Heaney. B–F, from Heaney *et al.* 2016a.

In this study, we explore the sources of variation in vertebral trabecular bone morphology of the Chrotomyini by quantifying the effects of body size, substrate use, intrataxonomic variation and evolutionary history on a variety of standard trabecular bone characteristics. We assess variation within species,

between species and between genera, and compare it to variation in other mammalian groups, as well as to the functional demands on mammalian trabecular bone across body size and ecology. We discuss the relative influence of each factor on vertebral trabecular bone, and track instances of apparent overlap in influence

from diverse sources. Finally, we examine how the long evolutionary history shared by these animals may influence how we interpret the functional significance of their trabecular bone morphology.

MATERIAL AND METHODS

SPECIES SELECTION, AND HABITAT AND SUBSTRATE USE

We sourced 67 specimens of 11 species of murine rodents belonging to the tribe Chrotomyini (sensu Rowsey et al., 2018) from the mammal collections of the Field Museum of Natural History (FMNH: Table 1). Our taxon sampling encompassed the breadth of body size and ecological diversity among the Chrotomyini, but is still tractable for sampling multiple specimens to assess intraspecific variation. The animals we sampled occur primarily in the higher-elevation habitats of the Philippine cloud forests, termed montane forest (~900 to 1600 m a.s.l. in elevation) and mossy forest (1600 to ~3000 m a.s.l.). Montane and mossy forest are characterized by trees mostly under 25 m tall, and a thick layer of humus on the ground surface (between 10 cm and 1 m; Fernando et al., 2008; Heaney et al., 2016a). Only two species included here (Apomys sierrae and Chrotomys mindorensis; Heaney et al., 1998, 2016a; Rickart et al., 2005; Justiniano et al., 2015) are

commonly found in lowland forest habitats (sea level to 900 m a.s.l. in elevation), where trees can reach 40 m in height and the layer of humus is missing, largely due to the activity of huge numbers of termites and ants (Heaney et al., 2016a).

The smallest animals in the sample are members of the genus Soricomys, which have a shrew-like body form and forage in leaf litter on the ground surface (Balete et al., 2012). The genus Archboldomys is morphologically and ecologically similar to Soricomys, such that until 2012 they were encompassed in a single genus (Balete et al., 2006, 2012). Archboldomys also forages in leaf litter on the ground surface. The genus *Apomys* (subgenus Megapomys; Heaney et al., 2011) is larger and more rat-like, and comprises at least 14 species, all of which are generalist ambulatory/terrestrial animals that forage on the ground surface (Heaney et al., 2011, 2016a). The three species in our sample capture the full body mass range within the subgenus *Megapomys* (Heaney et al., 2016a). In the genus Chrotomys, body mass can be more than twice that of Megapomys (Table 1). The three included species of *Chrotomys* all dig during foraging, but vary slightly in the intensity of this behaviour. Chrotomys silaceus and Chrotomys whiteheadi are more common in montane and mossy forests, and can be found digging in thick humus (Rickart et al., 2005; Heaney et al., 2016a). Chrotomys mindorensis is more common in lowland forest (Musser

Table 1. Body mass, habitat and substrate use of the species included here. Body mass values are mean values across individuals sampled in this study. M/F denotes how many specimens of each sex were included; i.e., 6 (3F/3M) means six specimens total, three male and three female

Genus	Species	N speci- mens	Mean mass (g, this study)	Habitat	Substrate use
Apomys	banahao	6 (3F/3M)	78.2	Montane to mossy forest	Terrestrial, forage on surface
Apomys	datae	6 (3F/3M)	67.8	Montane to mossy forest	Terrestrial, forage on surface
Apomys	sierrae	6 (3F/3M)	88.8	Lowland to montane and lower mossy forest	Terrestrial, forage on surface
Archboldomys	maximus	6 (2F/4M)	46.2	Montane to mossy forest	Terrestrial, forage in leaf litter
Chrotomys	mindorensis	6 (3F/3M)	173.7	Mostly lowland forest	Semifossorial, com- pact soil
Chrotomys	silaceus	7 (3F/4M)	108.7	Montane to mossy forest, more common at higher elevations	Semifossorial, humus
Chrotomys	whiteheadi	6 (3F/3M)	150.2	Montane to mossy forest	Semifossorial, humus
Rhynchomys	labo	6 (3F/3M)	164.3	Montane to mossy forest	Half-bound/hopping
Soricomys	kalinga	6 (3F/3M)	26.7	Montane to mossy forest	Terrestrial, forage on surface in leaf litter
Soricomys	leonardocoi	6 (3F/3M)	32.0	Montane to mossy forest	Terrestrial, forage on surface in leaf litter
Soricomys	montanus	6 (3F/3M)	24.8	Montane to mossy forest	Terrestrial, forage on surface in leaf litter

et al., 1982; Heaney et al., 2016a), where the thick layer of soft, uncompacted humus gives way to compact soil which requires more effort to displace. As a result, we consider *C. mindorensis* to be slightly more fossorial than its congeners, because it probably experiences more skeletal stress related to digging behaviours. It is important to note that although *Chrotomys* species are semifossorial, they are not subterranean: they mostly dig small pits or tunnels during foraging, which can be 0.5 to 1.5 animal body lengths (L. Heaney, pers. obs.). The final genus in the clade is *Rhynchomys*, members of which are similar in mass to large Chrotomys but have a highly distinct locomotor ecology (Musser & Freeman, 1981; Balete et al., 2007). They use their powerful hind legs for bounding or bipedal hopping and maintain surface trails for hunting and capturing earthworms (Heaney et al., 2016a; Rickart et al., 2019).

We chose at least six specimens per species (three females and three males). The only exceptions were *Archboldomys maximus*, for which only two adult females were available; we therefore included four males and two females; and *Chrotomys silaceus*, for which we sampled seven specimens (three females and four males). All specimens are fluid-preserved except a single dry skeleton of *Archboldomys maximus* (Supporting Information, Table S1). Only adults were used, as determined by body size and fusion of limb bone epiphyses. If there was any question regarding age, we also examined cranial suture fusion and dental wear, and excluded subadults. Body mass for each animal was taken from field notes.

μCT SCANNING

All specimens were scanned at the University of Chicago using a GE phoenix v | tome | x µCT (computed tomography) scanner, with a 240 kV X-ray tube. Each scan encompassed the entire lumbar spine at the highest possible resolution and differences in scanner settings were minimized across specimens of a given species. Scan resolution varied by less than 5.5 µm within each species; most species had a range of less than 3 µm among specimens (Supporting Information, Table S2). Relative resolution, i.e., width of an average trabecular element as measured in pixels (Sode et al., 2008), ranged from 4.3 to 7 in our data set, with a global mean of 5.5 px/tb. This value is in line with those of previous trabecular bone studies (Sode et al., 2008; Smith & Angielczyk, 2022). A high relative resolution was maintained in an attempt to reduce partial volume effects (PVE), a source of error resulting from the finite pixel binning in CT imaging (Soret et al., 2007), which can have large effects on small trabeculae (Kothari et al., 1999). We reconstructed scans in GE phoenix datos | x and aligned and cropped resulting image stacks in VGStudioMAX 3.3.

SEGMENTATION AND ISOLATION OF VERTEBRAL TRABECULAR BONE

Reconstructed slices were segmented in ORS Dragonfly 2021. We chose to focus on the trabecular bone of the lumbar spine because it is the most plastic region of the vertebral column (Jones et al., 2018), and lumbar spine gross morphology has a demonstrated correlation with locomotor mode in several mammalian groups (Boszczyk et al., 2001: Álvarez et al., 2013; Granatosky et al., 2014; Jones, 2015a, b). More broadly, the lumbar spine is critical to both mobility and support during mammalian locomotion (Slijper, 1946; Hildebrand, 1959, 1985; English, 1980), and therefore has the potential to reflect differences in mechanical environment related to locomotor style. We isolated the third lumbar vertebra (L3), which has been shown to approximate the mean shape within the lumbar series (Chen et al., 2005) (Fig. 2). Ninety-four percent of specimens had six lumbar vertebrae, where the vertebra we inspected (L3) was separated from the sacrum by three additional lumbar vertebrae (L4-6). In the remaining 6% (N = 4 specimens, each from a different species; Supporting Information, Table S1), three animals had five lumbar vertebrae, for which we inspected L3 (two positions away from the sacrum). For one specimen, the thoracic/lumbar split was unclear: the intervertebral joint at the cranial end of what would usually have been L1 (in an animal with six lumbar positions) had a rib on only one side (anatomical left). For this animal, we considered the vertebra with one rib to be a lumbar position, and its L3 was therefore in the same position relative to the sacrum as in specimens with six lumbar vertebrae.

In sagittal view, we manually traced every fifth slice through the medullary cavity of the vertebra, and produced a volume of interest (VOI) encompassing all the trabecular bone and intertrabecular space using the 'Interpolate' function in Dragonfly, referred to below as the total VOI. All specimens were traced by one author (SMS) to minimize interobserver error. After interpolation, the total VOI was inspected slice by slice to ensure that it accurately captured the entire medullary cavity. The VOI was smoothed once (kernel size = 9 px) and eroded once (kernel size = 3 px) to remove any errant cortical bone pixels around the margin (after Fajardo et al., 2007b, 2013). This resulted in removal of very small (~1-2 pixel) portions of the marrow space at the edges, and was visually inspected to ensure consistency across specimens. Using the resulting, finalized total VOI as a mask, we used the 'Segment with AI' function and a previously trained machine learning classifier (Smith & Angielczyk, 2022) to produce two additional VOIs: one including only bone pixels (trabecular bone VOI), and one including

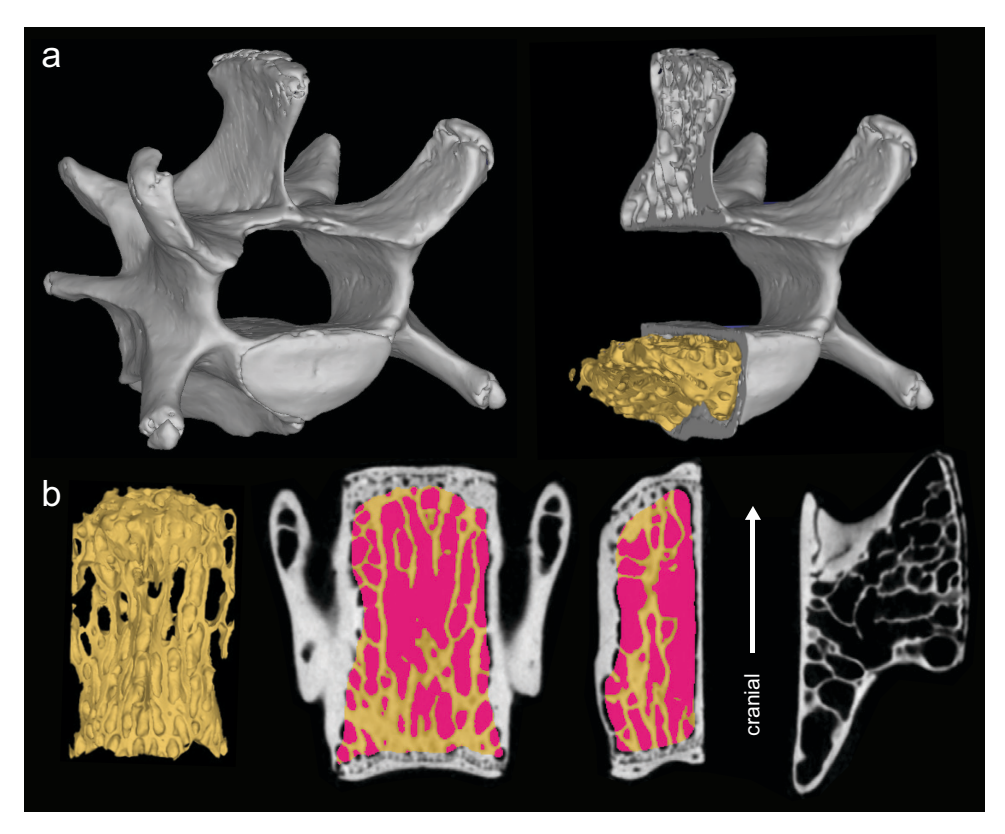


Figure 2. Segmentation of lumbar vertebrae for use in this study. A, Whole bone reconstruction of third lumbar vertebra (L03) of *Chrotomys whiteheadi* (FMNH 193744; left) and a longitudinal section showing the centrum trabecular bone we analyzed (right). B, 3D reconstruction of trabecular bone (left), with CT slices (middle, right) showing 2D slices of total volume of interest (VOI); coronal slice on left, sagittal on right. Bone is yellow, background is pink.

only background pixels (background VOI). We exported these VOIs as binary image stacks for analysis.

TRABECULAR BONE QUANTIFICATION

We collected four trabecular bone metrics on each sample: bone volume fraction (BV.TV), trabecular thickness (Tb.Th), trabecular separation (Tb.Sp) and connectivity density (Conn.D) (Fig. 3). We took trabecular bone volume directly from Dragonfly, as the volume of the trabecular bone VOI. We also measured total volume in Dragonfly, as the volume of the total VOI described above. Bone volume fraction was then calculated as a ratio: trabecular bone volume divided by total volume. Trabecular thickness, trabecular separation and connectivity density were calculated with the Fiji plugin BoneJ2 v.7.0.11 (Schindelin et al., 2012; Domander et al., 2021; Doube et al., 2021). For trabecular thickness, we used the binary image stack of bone pixels only (produced from the trabecular bone VOI). For trabecular separation, we used the binary image stack of background pixels only (produced from the background VOI) and the trabecular thickness command in BoneJ. This reduced the number of extraneous background pixels and made the trabecular separation measurement more accurate for the full medullary cavity (see Supporting Information, Fig. S1 for details). For the same reason, we used the binary image stack of bone pixels only to calculate connectivity in BoneJ, and then calculated connectivity density as connectivity divided by the volume of the total VOI, obtained from Dragonfly (Figs 2, 3). To assess the basic relationships among trabecular bone metrics, we calculated pairwise Pearson correlations using the R stats package (R Core Team, 2022). We compared the variability of metrics using coefficient of variation (CV), which expresses standard deviation as a proportion of the mean, making it effective for comparing metrics with very different magnitudes. We also executed principal components ordination on standardized trabecular bone metrics and body mass.

MOLECULAR METHODS AND PHYLOGENETIC INFERENCE

We sampled molecular data from members of Chrotomyini (11 individuals representing 11 species),

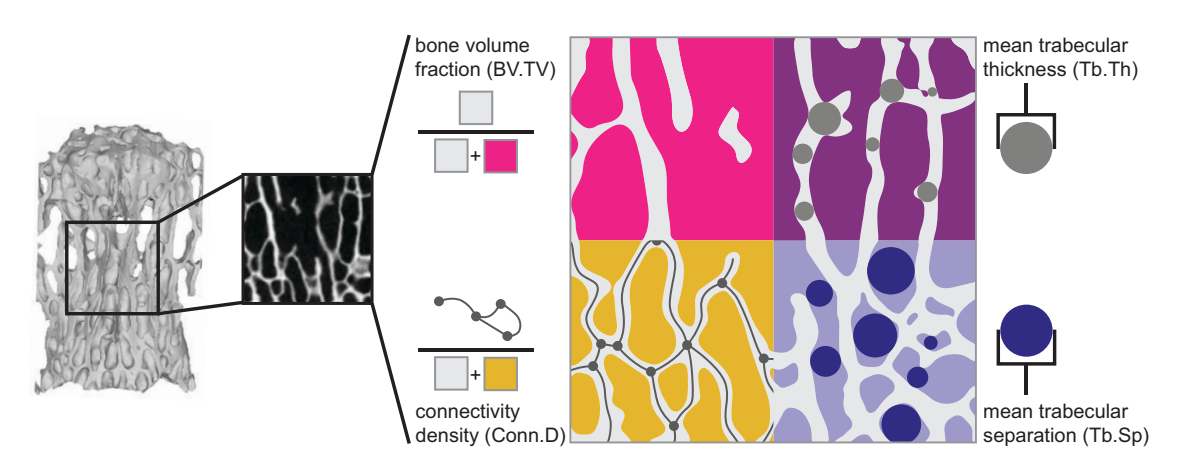


Figure 3. Trabecular bone metrics measured in this study, as shown on a 2D slice of trabecular bone. Bone volume fraction is a ratio and is therefore unitless; connectivity density is a scalar per unit volume and is measured in mm⁻³; trabecular thickness and trabecular separation are measured in mm. All metrics are measured in three dimensions and are shown here as 2D projections. In bone volume fraction and connectivity density depictions, grey boxes represent bone volume; pink and yellow boxes represent nonbone volume (background).

and other related murine rodents (14 individuals representing 14 species) to provide phylogenetic context for our morphological analyses. We analysed sequence data from eight total loci, including: mitochondrial gene cytochrome b [Cytb; 1144 base pairs (bp)], nuclear intron 3 of benzodiazepine receptor (Bdr; 1030 bp), intron 7 of beta-fibringen (Fgb7; 840 bp), intron 3 of opsin (Opn, an X-linked locus; 1547 bp), exon 10 of growth hormone receptor (Ghr; 915 bp), exon 1 of interphotoreceptor retinoid binding protein (Rbp3;1434 bp), a portion of the single exon of recombination activating gene 1 (Rag1; 2097 bp) and exon 11 of breast cancer associated 1 gene (BRCA1; 2668 bp). Sequences were obtained from GenBank, supplemented by new sequences generated from specimens held at FMNH to expand available sequence information for Chrotomys mindorensis, Rhynchomys labo and Soricomys kalinga. DNA extraction, amplification and sequencing protocols were conducted as described in Rowsey et al. (2022). In total, we generated 12 new sequences (submitted to GenBank with accession numbers OQ630973-OQ630984). Our final concatenated sequence alignment included 25 individuals and 11 342 bp (Supporting Information, Table S3).

We used PartitionFinder v.2.1.1 (Lanfear *et al.*, 2012) to determine a best-fit nucleotide substitution model partitioning scheme, specifying candidate partition schemes by locus, and evaluated support using the Bayesian information criterion (Schwarz, 1978). Candidate models included those supported by BEAST. *Cytb* lacked the information content necessary to achieve convergence for transversion rates under a GTR substitution model (Gu *et al.*, 1995) and we thus used a TN93 model (Tamura & Nei, 1993) for this locus. The best-fit nucleotide substitution partitioning

scheme is reported in Supporting Information, Table S4. We performed a Bayesian concatenated phylogenetic analysis using BEAST v.2.6.6 as implemented in the CIPRES Science Gateway (Miller et al., 2010; Bouckaert et al., 2014, 2019). We calibrated the phylogenetic analysis in absolute time using secondary calibration points from Rowsey et al. (2018), based on fossil data from Kimura et al. (2015) to specify normal clade age priors for several nodes in the tree: the crown age of Chrotomyini (as given by the most recent common ancestor of Apomys and all other members of Chrotomyini: mean: 7.22 Mya, SD: 0.506); the crown age of Phloeomyini (as given by the most recent common ancestor of Crateromys schadenbergi and Phloeomys pallidus: mean: 11.1 Mya, SD: 0.825), the crown age of Rattini (as given by the most recent common ancestor of Micromys minutus and Rattus norvegicus: mean: 8.82 Mya, SD: 0.660) and the root of the tree (mean: 20.65 Mya, SD: 1.21). We specified nucleotide substitution models according to the PartitionFinder best-fit scheme and modelled separate, relaxed log-normal molecular clocks for the mitochondrial and nuclear loci, where the nuclear clock rate was estimated relative to the rate of the mitochondrial clock (held at 1.0), to facilitate Markov-Chain Monte Carlo optimizer convergence [defined as an estimated sum of squares (ESS) value ≥ 200 for all parameters]. We additionally specified a Yule branching model for our tree prior (Yule, 1924), with an exponential prior for birth rate. All other priors were given default values. We ran the phylogenetic analysis for 1.0 × 108 generations, sampling trees every 2.0×10^5 generations. We retained 4500 trees after discarding 10% as burn-in, and generated a maximum clade credibility (MCC) tree using TreeAnnotator

v.2.6.0 (Bouckaert *et al.*, 2014, 2019) based on median node heights for use in our phylogenetic comparative analyses. The final tree was pruned to exclude non-focal taxa prior to phylogenetic multilevel model analysis (full tree available in Supporting Information, Fig. S2).

BAYESIAN PHYLOGENETIC MULTILEVEL MODELS

We assessed trabecular bone differences among substrate use types, and measured the effects of phylogenetic non-independence and body mass, using Bayesian phylogenetic and non-phylogenetic multilevel models. In each analysis, one trabecular bone metric (bone volume fraction, trabecular thickness, trabecular separation or connectivity density) was used as the response variable. Taxon (either genus or species, see below) and log10-transformed body mass (in grammes) were used as population-level predictors. In one set of models, phylogenetic history of these species was used as a group-level predictor (Hadfield & Nakagawa, 2010; Villemereuil & Nakagawa, 2014; Bürkner, 2021), using the correlation matrix from the tree inferred here. In the other set of models, no phylogenetic information was included. We standardized both trabecular bone metrics and mass to have a mean of 0 and standard deviation of 1 prior to analysis, and used normal regularizing priors on all populationlevel effects to prevent overfitting [Normal (0,1); McElreath, 2020]. We executed analyses in R 4.1.3 (R Core Team, 2022) with brms v.2.17.0 (Bürkner, 2017, 2018, 2021) which uses the probabilistic programming language Stan (Carpenter et al., 2017). Each model was run with four chains for 2000 iterations, including 50% burn-in, for a total of 4000 posterior samples. Acceptable convergence was demonstrated with R < 1.01. We estimated phylogenetic signal with the multilevel-model estimate of Pagel's lambda (Hadfield & Nakagawa, 2010; Villemereuil & Nakagawa, 2014).

ALLOMETRY

We executed phylogenetically-informed allometry analysis on each trabecular bone metric using brms (Bürkner, 2017). For allometry models, we used nonstandardized data and log-10 transformed mass (grammes), trabecular thickness (mm), trabecular separation (mm) and connectivity density (mm⁻³). We did not log-transform bone-volume fraction (a unitless ratio). We also eliminated taxon as a predictor. These methodological choices allow us to reasonably compare our results to those of other trabecular bone allometry studies (e.g., Doube *et al.*, 2011; Fajardo *et al.*, 2013; Mielke *et al.*, 2018; Webb, 2021). In each analysis, one trabecular bone metric (bone volume fraction, trabecular thickness, trabecular separation or connectivity density) was used as the response

variable, and log10-transformed body mass was used as the population-level predictor. As in the models above, we incorporated our phylogeny as a group-level predictor (Hadfield & Nakagawa, 2010; Villemereuil & Nakagawa, 2014; Bürkner, 2021), and used a normal regularizing prior on the population-level predictor [Normal (0,1); McElreath, 2020]. Each model was run with four chains for 2000 iterations, including 50% burn-in, for a total of 4000 posterior samples. Acceptable convergence was demonstrated with $\hat{R} < 1.01$.

Our expectations for isometry largely correspond to those used in previous work (e.g., Fajardo et al., 2013; Mielke et al., 2018; Zack et al., 2023). For bone volume fraction, we considered an allometric scaling coefficient of $\alpha = 0$ to be isometric, as bone volume fraction is a ratio (mm³/mm³) and the dimensions therefore cancel out. For trabecular thickness and trabecular separation, we considered $\alpha = 0.33$ to be isometric, because both are measures of length (mm) and therefore scale at 1/3 relative to volume and mass. For connectivity density, we considered $\alpha = -1.00$ to be isometric, because it is a scalar (connectivity) divided by a volume (mm⁻³), and volume scales 1/1 with mass. Following the suggestions of McElreath (2020), if the 89% credible interval of the model estimate for slope (α) did not include the predicted value for isometry, we considered the relationship to be allometric.

RESULTS

RAW TRABECULAR BONE CHARACTERISTICS ACROSS SPECIES

Mean raw values for each of the four trabecular bone metrics we examined are shown in Table 2 (individual values in Supporting Information, Table S1). The bone volume fraction for all species falls between 19.5% (Soricomys leonardocoi) and 33.8% (Chrotomys whiteheadi). Chrotomys mindorensis is a close second for maximum bone volume fraction (33.7%). Soricomys montanus has the thinnest trabeculae on average (0.066 mm) but S. kalinga has the smallest trabecular separation (0.251 mm). Chrotomys mindorensis has the thickest trabeculae on average (0.133 mm) and the largest trabecular separation (0.351 mm). Soricomys montanus and C. mindorensis also represent the extremes of connectivity density: S. montanus connectivity density is the highest, at 59.08 mm⁻³, and C. mindorensis connectivity density is lowest, at 11.94 mm⁻³. These raw results clearly indicate the effects of body size on trabecular bone metrics, as S. montanus is the smallest species in the dataset (mean mass = $24.8 \,\mathrm{g}$), and *C. mindorensis* is the largest (mean mass = 173.7 g; Table 1).

Table 2. Species means of raw trabecular bone metrics. Numbers in parentheses are CV, i.e., standard deviation
expressed as a proportion of the mean

Genus	Species	N	Bone volume fraction (BV.TV)	Trabecular thickness (Tb.Th, mm)	Trabecular separation (Tb.Sp, mm)	•
Apomys	banahao	6	0.277 (0.152)	0.0974 (0.0629)	0.281 (0.110)	35.61 (0.20)
Apomys	datae	6	$0.233\ (0.155)$	$0.0918\ (0.0565)$	0.340 (0.168)	21.60 (0.39)
Apomys	sierrae	6	$0.296\ (0.236)$	0.0985 (0.0606)	0.280 (0.254)	34.52(0.77)
Archboldomys	maximus	6	0.201(0.229)	0.0777 (0.0923)	0.302(0.285)	38.98 (0.61)
Chrotomys	mindorensis	6	$0.337\ (0.122)$	$0.133\ (0.058)$	0.351(0.157)	11.94 (0.30)
Chrotomys	silaceus	7	0.241(0.066)	0.100 (0.120)	0.348 (0.147)	32.33 (0.51)
Chrotomys	whiteheadi	6	0.338(0.175)	0.123 (0.090)	0.317 (0.142)	16.61 (0.48)
Rhynchomys	labo	6	0.243 (0.086)	0.112 (0.046)	0.380 (0.187)	22.07 (0.34)
Soricomys	kalinga	6	$0.240\ (0.104)$	0.0720(0.0681)	0.251 (0.088)	57.43 (0.39)
Soricomys	leonardocoi	6	0.195 (0.159)	0.0719(0.0292)	0.330 (0.236)	56.79 (0.37)
Soricomys	montanus	6	$0.216\ (0.227)$	0.0666(0.0478)	$0.267\ (0.225)$	59.08 (0.37)

CV, which is standard deviation expressed as a percentage of the mean (Table 2), shows that intraspecific variation is highest in connectivity density (with standard deviation representing up to 77% of the mean, in *Apomys sierrae*). In contrast, CV is especially low in trabecular thickness, with ten of 11 species having CVs less than 0.1. For bone volume fraction and trabecular separation, CVs fall mostly between 0.1 and 0.25. In addition to having the highest intraspecific variation for connectivity density, *Apomys sierrae* has the highest CV for bone volume fraction as well (0.236). *Chrotomys silaceus* is the most variable species in trabecular thickness (CV = 0.120), and *Archboldomys maximus* is the most variable species in trabecular separation (CV = 0.285).

In our principal components analysis (PCA, Fig. 4), PC1 represents 62.14% of variation and has strong vector components for trabecular thickness and mass (higher at low values on PC1), and connectivity density (higher at high values on PC1). PC1 also captures intergeneric variation, which is related to body size: Soricomys and Archboldomys are small and have generally high PC1 scores, whereas Chrotomys and Rhynchomys are larger and have low PC1 scores. PC2 represents 29.88% of variation, and in contrast to PC1, captures intrageneric variation. This axis is dominated by strong vector components for bone volume fraction (high at higher values on PC2) and trabecular separation (high at lower values on PC2).

Figure 4 highlights some unusually distinct specimens that likely have an outsized effect on CV. One each of *Apomys sierrae* and *Archboldomys maximus* are separate from the main grouping of their taxon in the principal component space. The specimen of *Archboldomys maximus* (FMNH 193526) is distinguished from its conspecifics by its high trabecular separation, whereas the specimen of *Apomys*

sierrae (FMNH 216435) has a combination of high connectivity density and high bone volume fraction (Fig. 4 insets; Supporting Information, Table S1). Two specimens of Soricomys also fall relatively far away from their conspecifics (FMNH 188313, S. montanus, and 190968, S. leonardocoi). These two specimens share characteristics with FMNH 193526 (high trabecular separation and low bone volume fraction). but their morphology is not quite as extreme as that of FMNH 193526. We carefully examined each of these outliers to reassess age and health, and examined field notes for each to determine if there were any unusual circumstances surrounding their capture. These examinations confirmed that all specimens were adult and healthy, were caught in typical circumstances and were processed normally.

As has been demonstrated in a previous work (Goulet et al., 1994), trabecular bone metrics are correlated with one another (Table 3, Fig. 4). All possible pairings of the four metrics have significant Pearson correlation values (P < 0.05), except bone volume fraction and connectivity density, which is also the pairing with the smallest magnitude correlation coefficient (-0.16). In general, bone volume fraction is positively correlated with trabecular thickness and negatively correlated with trabecular separation, whereas connectivity density is negatively correlated with both. The strongest correlations are between bone volume fraction and trabecular thickness (coeff = 0.68), and connectivity density and trabecular thickness (coeff = -0.71).

PHYLOGENETIC ANALYSIS

The best-fit nucleotide partition scheme supported four partitions (Supporting Information, Table S4). The maximum clade credibility tree provides the

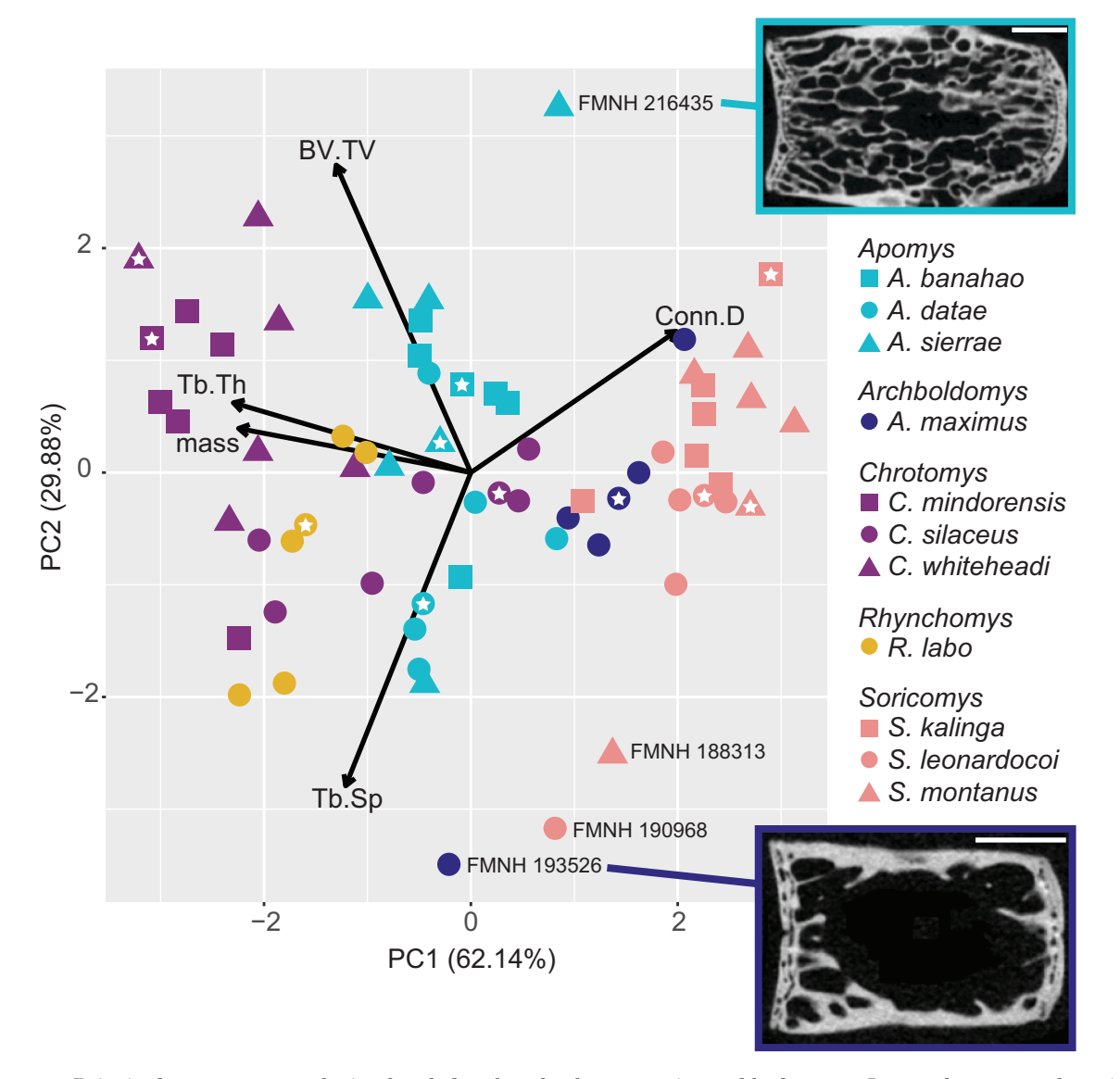


Figure 4. Principal component analysis of scaled trabecular bone metrics and body mass. Insets show coronal sections through the third lumbar vertebrae of two outliers: FMNH 216435 ($Apomys\ sierrae$) and FMNH 193526 ($Archboldomys\ maximus$) (white scale bars = 1 mm). White stars denote points representing the specimens shown in Fig. 8, one specimen per species. BV. TV = bone volume fraction; Tb.Th = trabecular thickness; Tb.Sp = trabecular separation; Conn.D = connectivity density.

first sequence data obtained from $R.\ labo$, which is recovered as sister to Chrotomys and Soricomys with strong support, and consistent with other recent phylogenetic analyses of this group (e.g. Rowsey et al., 2018, 2022; Rowe et al., 2019; Fig. 5; Supporting Information, Fig. S2). All nodes were recovered with strong support (posterior probability ≥ 0.95) aside from the position of Apomys banahao relative to the other two species of Apomys included in the analysis. Divergence dates are largely consistent with prior studies, likely because we used a large number of node-age calibrations relative to the number of tips on

the tree (Rowsey *et al.*, 2018, 2022; Rowe *et al.*, 2019; Fig. 5; Supporting Information, Fig. S2).

BAYESIAN MULTILEVEL MODELS AND SUBSTRATE USE

Overall results of our Bayesian multilevel models across genera and species are shown in Figs. 6 and 7. Full model outputs are available in Supporting Information, Tables S5, S6. Across all models, the inclusion of phylogenetic covariance as a group-level predictor increases the uncertainty in estimates of

Table 3. Pairwise Pearson correlation between trabecular bone metrics. Asterisks denote correlations with P < 0.05. Numbers in parentheses are 89% confidence intervals for the listed estimate

	Trabecular thickness (Tb.Th, mm)	Trabecular separation (Tb.Sp, mm)	Connectivity density (Conn.D, 1/mm ⁻³)
Bone volume fraction (BV.TV) Trabecular thickness	0.68 (0.57–0.78)*	-0.34 (-0.510.16)* 0.36 (0.18-0.52)*	-0.16 (-0.34–0.35) -0.71 (-0.80– -0.61)*
(Tb.Th, mm)		0.80 (0.10 0.82)	,
Trabecular separation (Tb.Sp, mm)	_	_	-0.63 (-0.74– -0.50)*

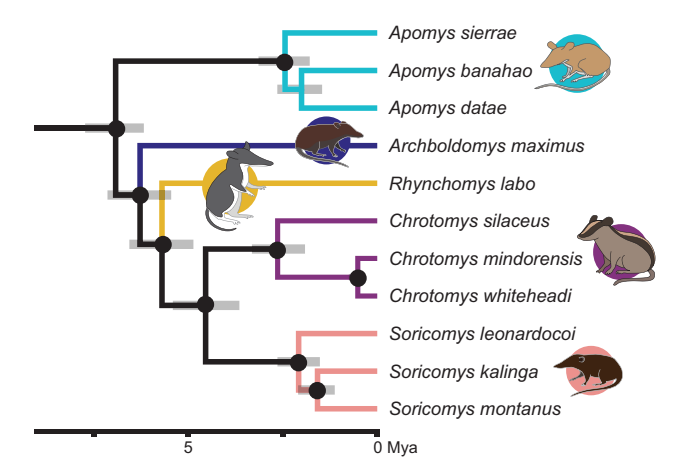


Figure 5. Pruned maximum clade credibility tree of Chrotomyini inferred using BEAST (full tree in Supporting Information, Fig. S1). Dots at nodes represent relationships inferred with strong support (posterior probability ≥ 0.95). Bars at nodes represent 95% highest posterior density interval of divergence date inferred from the posterior distribution of 4500 trees. Branches are colour-coded within each genus.

taxon mean, but, for most metrics, has relatively little effect on their positions relative to the global mean (0.0, shown by the horizontal dotted lines in Figs. 6, 7). Phylogenetic covariance structure has the largest effect on the position of taxonomic means in the genuslevel models for bone volume fraction and trabecular thickness, which are also the analyses with the highest estimated values for lambda (Fig. 6, Table 5). In species-level models (Fig. 7), probability distributions for lambda have stronger peaks at lower values than in genus-level models, suggesting a reduction in the influence of phylogeny on the estimates. Yet it is also notable that the distribution for lambda in the species-level analysis of trabecular thickness has two relatively low, broad peaks, one just above 0 and one just above 0.75 (estimated at 0.42, Table 5). This indicates that the model in this case cannot clearly distinguish phylogenetic sources of variation from other sources of variation.

At both genus- and species-level, the hopping Rhynchomys deviates the most from the mean bone volume fraction, with values that are much lower than would be expected given its body size (Figs 6, 7). Rhynchomys also has the highest trabecular separation and lowest trabecular thickness in the genus-level models. In species-level models, Archboldomys maximus (terrestrial, leaf-litter foraging) and *Chrotomys silaceus* (humus digging) have similar low trabecular thickness. Soricomys leonardocoi (terrestrial, leaf-litter foraging) and Apomys datae (terrestrial, surface foraging) have similar high trabecular separation. Chrotomys mindorensis (compact soil digging) is a standout in trabecular thickness, with much thicker trabeculae than expected for its body size: C. whiteheadi (humus digging) also has relatively thick trabeculae, though to a slightly lesser degree (Fig. 7, 8). Chrotomys silaceus has much thinner trabeculae; as noted above, it falls close to R. labo, with values below the global mean. Of the other two genera that are represented by multiple species (Soricomys and Apomys), neither has the wide intrageneric variation in trabecular thickness seen in Chrotomys. However, in all three of the other metrics, Apomys has striking intrageneric variation, and Soricomys shows substantial intrageneric variation in bone volume fraction and trabecular spacing. Intrageneric variation of connectivity density is higher in Apomys than in any other genus; this metric shows comparatively little variation in Soricomys and Chrotomys.

BODY MASS AND ALLOMETRY

As suggested by the raw data, body mass has a strong effect on the trabecular bone metrics we measured when considered in our Bayesian models (Table 4; Supporting Information, Tables S5, S6). The population-level effect of mass is strongest in trabecular thickness [β mass = 0.95 (89% credible interval = 0.68, 1.21) in genus-level analyses and 0.86 (0.61, 1.12) in species-level analyses], followed closely by bone volume fraction and connectivity

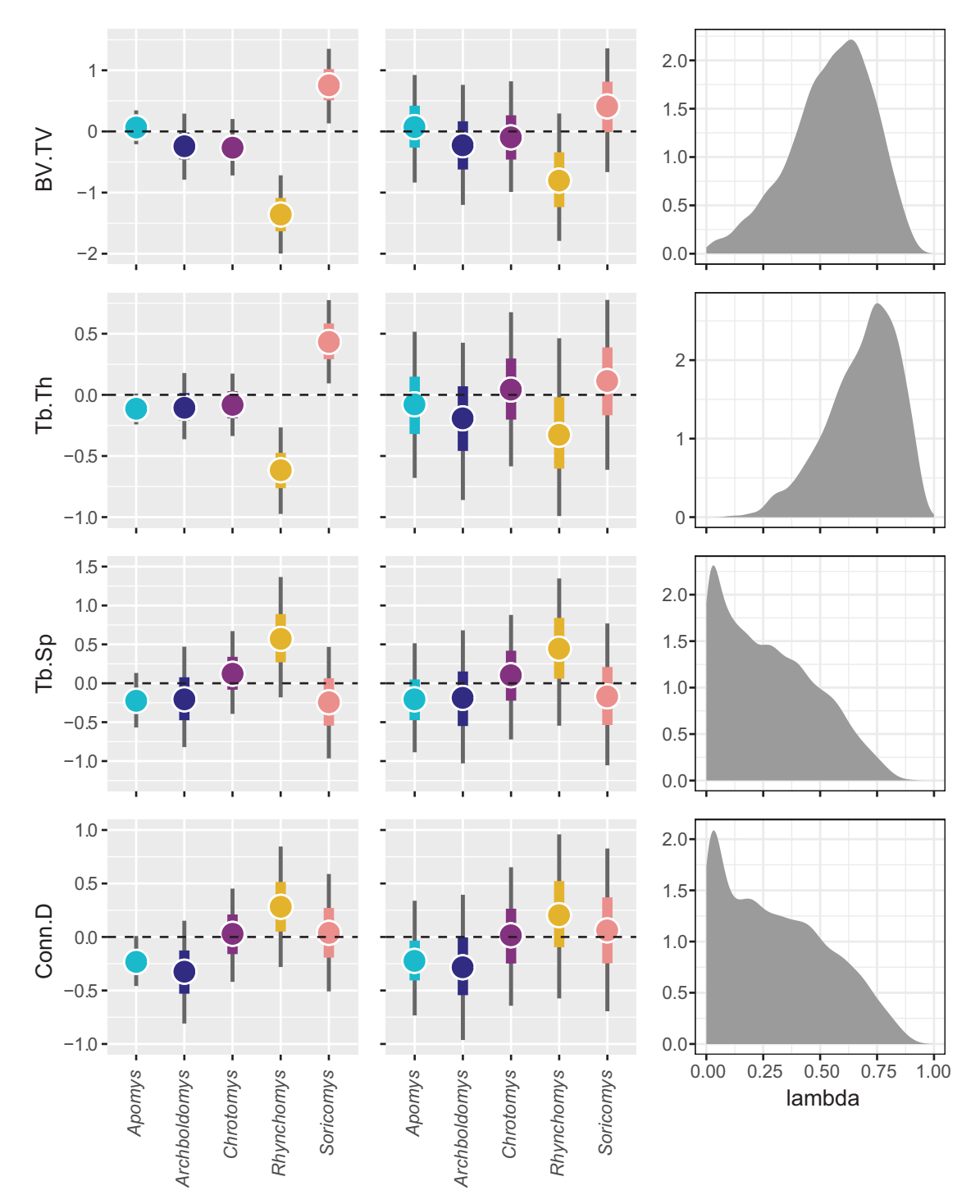


Figure 6. Posterior probability distributions for trabecular bone metrics by genus. Round points represent estimated genus mean. Thick coloured bars are 50% credible intervals; thin grey bars are 89% credible intervals. Horizontal line indicates global mean (0.0). Left column: posterior distributions for models without inclusion of phylogenetic correlation structure. Centre column: posterior distributions for models including phylogenetic correlation structure as a group-level predictor. Right: posterior probability distributions for lambda, from the same models as the centre column; y-axis = density. BV.TV = bone volume fraction; Tb.Th = trabecular thickness; Tb.Sp = trabecular separation; Conn.D = connectivity density.

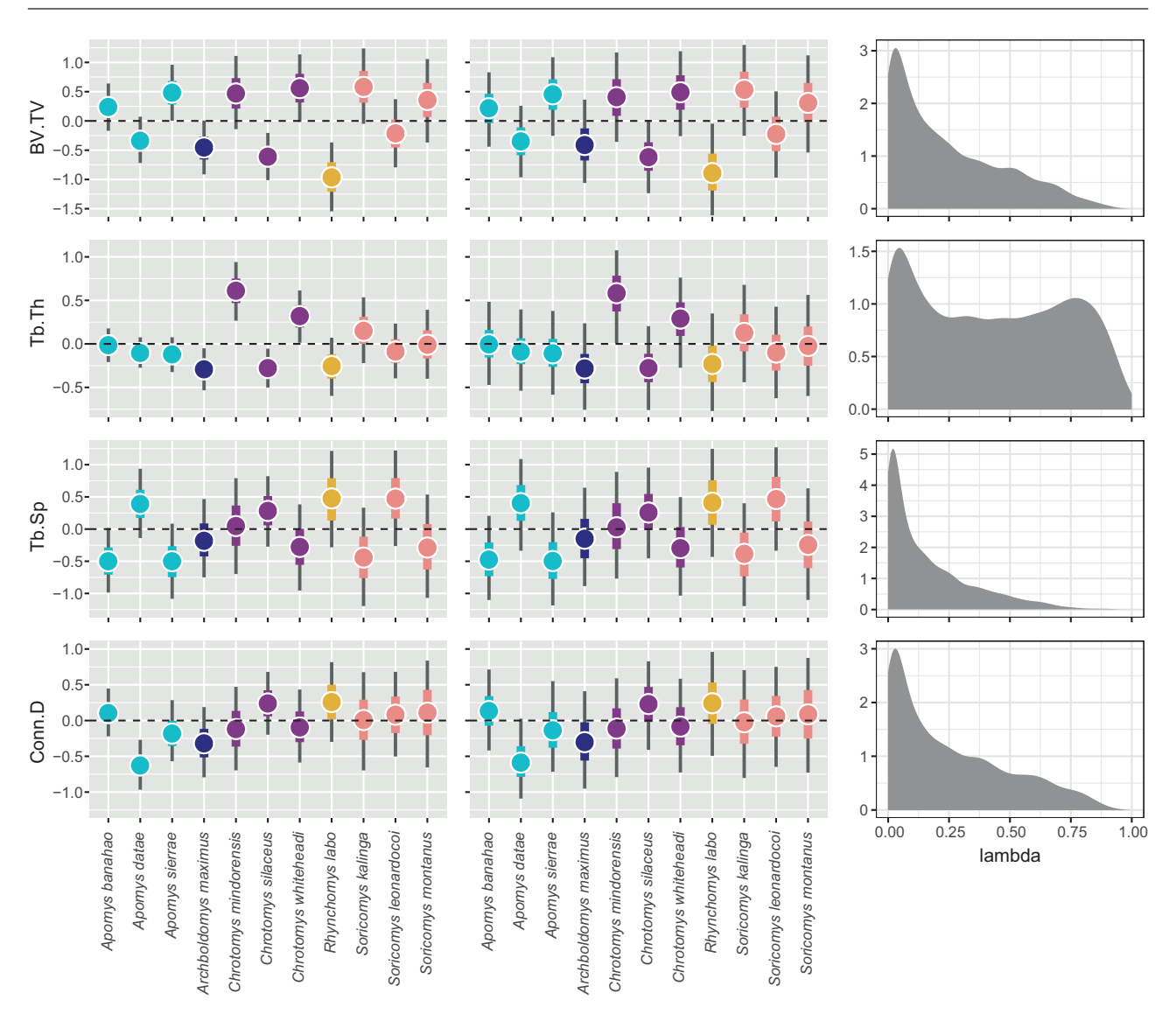


Figure 7. Posterior probability distributions for trabecular bone metrics by species. Round points represent estimated species mean. Thick coloured bars are 50% credible intervals; thin grey bars are 89% credible intervals. Horizontal line indicates global mean (0.0). Left column: posterior distributions for models without inclusion of phylogenetic correlation structure. Centre column: posterior distributions for models including phylogenetic correlation structure as a group-level predictor. Right: posterior probability distributions for lambda, from the same models as the centre column; y-axis = density. BV.TV = bone volume fraction; Tb.Th = trabecular thickness; Tb.Sp = trabecular separation; Conn.D = connectivity density.

density. The effect of mass on trabecular spacing is relatively weak however [$\beta mass = 0.27 \ (-0.22, 0.77)$ in genus-level analyses and 0.34 (-0.11, 0.79) in species-level analyses]. We found slight positive allometry in bone volume fraction, with an estimated allometric coefficient (α) of 0.14 (0.07, 0.22), compared with a prediction of α = 0 at isometry (Table 4, Fig. 9). Connectivity density also exhibits positive allometry [α = -0.72 (-0.99, -0.50) vs. -1 at isometry]. Trabecular thickness scales isometrically [α = 0.30 (0.25, 0.34), with isometry at 0.33] and trabecular separation

scales with slight negative allometry [$\alpha = 0.12$ (0.03, 0.25), with isometry at 0.33].

DISCUSSION

BONE VOLUME FRACTION ALLOMETRY AND SMALL BODY SIZE

The scaling patterns in our data, i.e., which trabecular bone metrics increase and decrease in relation to body size, broadly correspond to patterns recovered

Table 4. Effects of mass. Values for beta are for models using genus or species and mass as predictors. Allometry estimates are from models using only mass as predictor. All models include phylogenetic covariance as a group-level effect. Numbers in parentheses are 89% credible intervals for the listed estimate. Bayesian R^2 values calculated with the function bayes_ R^2 in brms

	Population-level	effects	Allometry			
	βmass, genus	βmass, species	Estimated α	${f R}^2$	Isometry	Allometry
Bone volume fraction (BV.TV)	0.81 (0.34–1.27)	0.66 (0.26–1.06)	0.14 (0.07–0.22)	0.57 (0.46–0.65)	$\alpha = 0$	pos
Trabecular thickness (Tb.Th, mm)	0.95 (0.68–1.21)	0.86 (0.61–1.12)	0.30 (0.25–0.34)	0.93 (0.92–0.94)	$\alpha = 0.33$	iso
Trabecular separation (Tb.Sp, mm)	0.27 (-0.22–0.77)	0.34 (-0.11–0.79)	0.12 (0.03–0.25)	0.26 (0.12–0.39)	$\alpha = 0.33$	neg
Connectivity density (Conn.D, 1/mm ⁻³)	-0.72 (-1.13– -0.30)	-0.73 (-1.140.34)	-0.72 (-0.99– -0.50)	0.53 (0.42–0.62)	α = -1	pos

Table 5. Estimates of phylogenetic signal (lambda). Values for trabecular bone metrics are for models using genus or species and mass as predictors. Value for mass is for model using the default brms intercept and no additional predictors. All models include phylogenetic covariance as a group-level effect. Numbers in parentheses are 89% credible intervals for the listed estimate

	Model		
	Species	Genus	
Bone volume fraction (BV.TV)	0.24 (0-0.68)	0.56 (0.24–0.81)	
Trabecular thickness (Tb.Th, mm)	0.42 (0.01-0.88)	0.69 (0.41-0.90)	
Trabecular separation (Tb.Sp, mm)	0.17 (0-0.55)	0.21 (0-0.63)	
Connectivity density (Conn.D, 1/mm ⁻³)	0.24 (0-0.70)	0.30 (0.01-0.70)	
Mass (log grammes)	0.96 (0.92-0.98)		

in previous studies of trabecular bone from various clades and anatomical sites (Fajardo et al., 2013; Ryan & Shaw, 2013; Mielke et al., 2018; Saers et al., 2019; Amson & Bibi, 2021; Webb, 2021; Zack et al., 2023). We found that absolute trabecular thickness and separation increase with increasing body mass, and connectivity density decreases with increasing body mass (Table 4, Fig. 9). Larger animals in our sample therefore have absolutely thicker trabeculae, with absolutely larger spaces between them, and fewer connections among them.

We also found a relationship between bone volume fraction and body mass, wherein the trabeculae of larger animals occupy an absolutely greater amount of available space than those of smaller animals. In the case of bone volume fraction, this amounts to a positively allometric relationship. At isometry, the predicted slope of the relationship between bone volume fraction and body mass is 0, because bone

volume fraction is a scalar and therefore has no inherent relationship with size metrics. We found the slope of this relationship to be greater than 0 (Fig. 9, Table 4), indicating that in the body size range we examined, larger animals also have a relatively higher bone volume fraction than expected for their body size (Table 4). The signal here is slight ($\alpha = 0.14$), but the 89% credible intervals exclude 0, and our Bayesian R² value is comparatively high at 0.57 (Table 4). Other studies show similar allometric coefficients for bone volume fraction, but tend to have low R2 values, suggesting that the relationship is weak (Ryan & Shaw, 2013: $R^2 = 0.38$; Webb, 2021: $R^2 = 0.11$). Doube et al. (2011) found an allometric scaling coefficient of 0.201 for bone volume fraction, but an R2 of 0.049, and they therefore reported no relationship between mass and bone volume fraction.

Increasing bone volume fraction with body mass makes theoretical biomechanical sense. Under

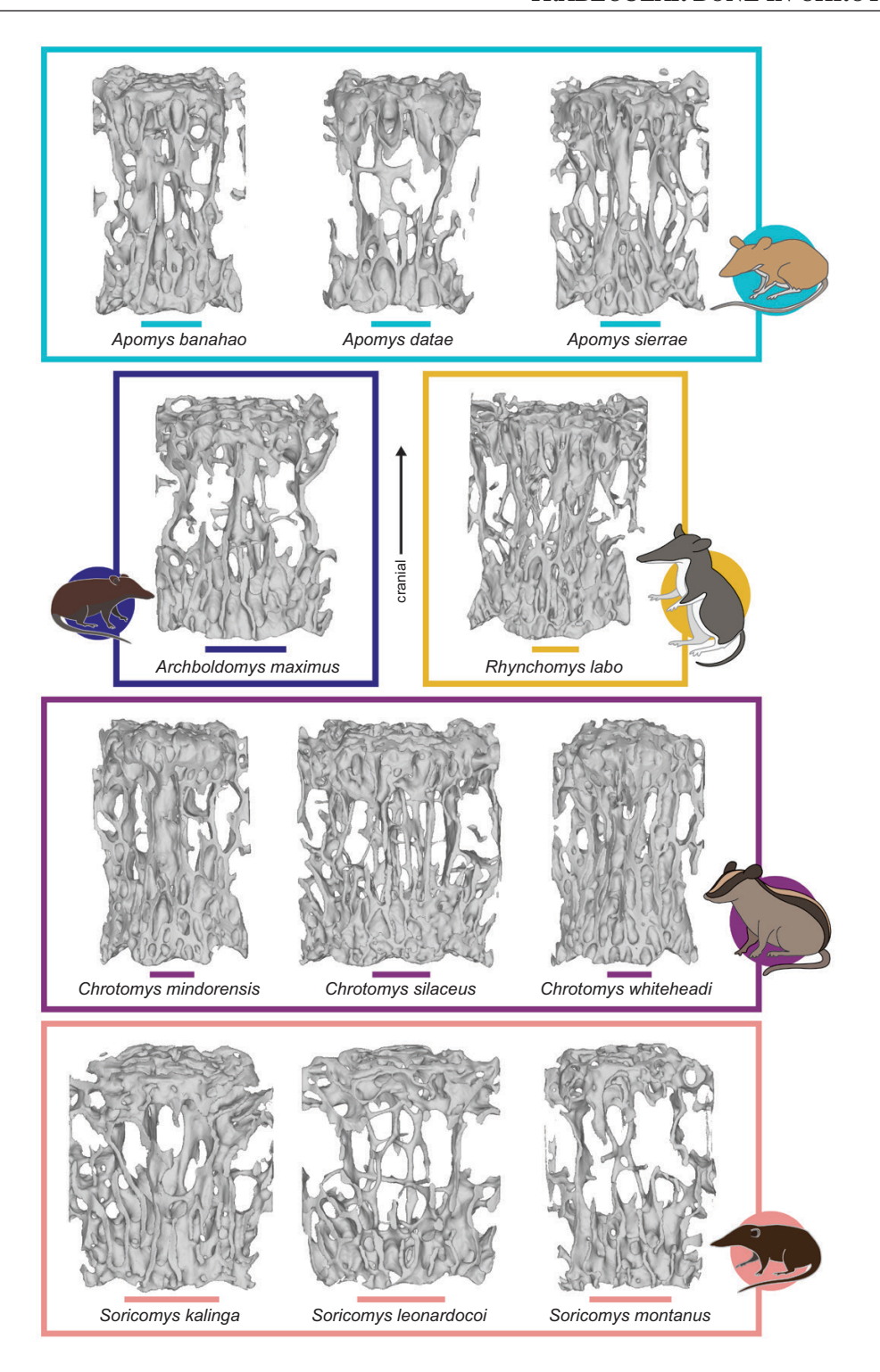


Figure 8. Representative trabecular bone volumes of interest (VOIs) from each included taxon. VOIs include the entire medullary cavity (see Methods for segmentation details). All models are displayed in ventral view with cranial towards the top of the figure. Trabeculae that appear floating connect only to the cortical bone and do not intersect with other trabeculae. Scale bars below each specimen are 1 mm. Field Museum (FMNH) specimen numbers are as follows: *Apomys banahao*, 218302; *Apomys datae*, 236309; *Apomys sierrae*, 216432; *Archboldomys maximus*, 193524; *Rhynchomys labo*, 189833; *Chrotomys mindorensis*, 221843; *Chrotomys silaceus*, 193726; *Chrotomys whiteheadi*, 193744; *Soricomys kalinga*, 167307; *Soricomys leonardocoi*, 190962; *Soricomys montanus*, 193519. Location of each specimen on the principal component plot in Fig. 4 is denoted by a white star.

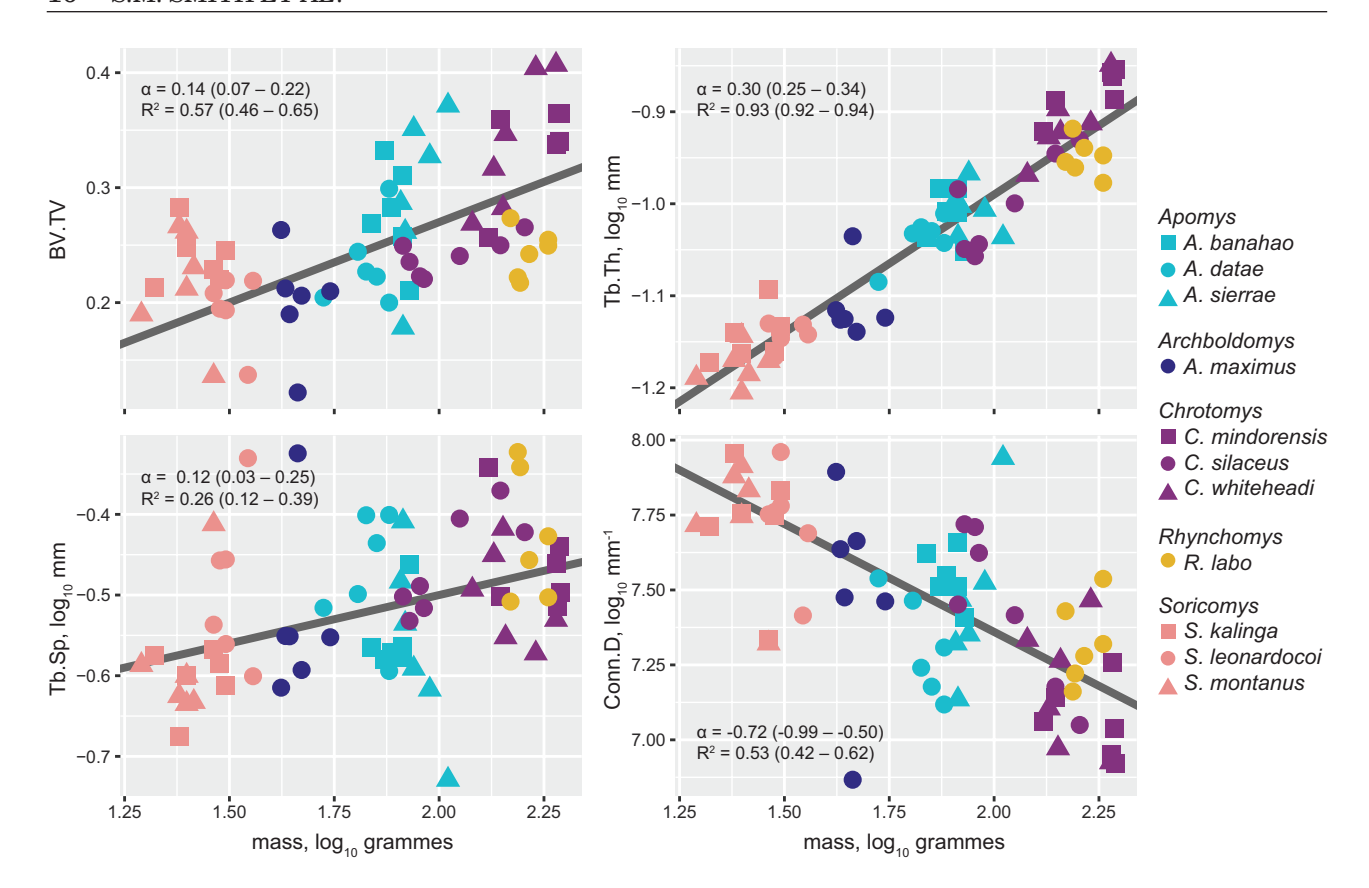


Figure 9. Plots of allometric scaling relationships in trabecular bone metrics. Estimates for α and Bayesian R2 values are also listed in Table 4. All are from models using only mass as a predictor, and including phylogenetic covariance as a group-level effect. Numbers in parentheses are 89% credible intervals for the listed estimate. BV.TV = bone volume fraction; Tb.Th = trabecular thickness; Tb.Sp = trabecular separation; Conn.D = connectivity density.

geometric similarity, the ability of a bone to withstand stress (related to cross-sectional area, in units of length²) decreases relative to the stress imparted by increasing body mass (proportional to volume, in units of length³) (Christiansen, 1999). Higher bone volume fraction corresponds to higher yield stress (Bevill & Keaveny, 2009), and would therefore be one way to meet the mechanical demands of larger body mass. Yet there are limits to how much bone volume fraction can realistically increase. As a ratio, it cannot exceed 1, but physiological constraints prevent trabecular bone from coming close to this density. Osteocyte demands on nutrient diffusion (Lozupone & Favia, 1990; Doube et al., 2011) and the increasing mass associated with denser bone constrain trabecular density. Unable to make their limb bones denser to address the functional demands of larger body size, quadrupedal mammals are hypothesized to have instead evolved postural changes (Biewener, 1989, 1990). Such changes may not be required at small body size: it has been hypothesized that at body masses under about 100 g, bone gross morphology will scale isometrically due to selection

favouring bone stiffness instead of failure strength at that size (Biewener, 1990: table 1).

The hypothesis that there are different selective pressures on the skeleton at small body sizes may extend to scaling relationships in trabecular bone. This possibility was noted previously in a literature meta-analysis (Barak et al., 2013), which found that variation in the bone volume fraction of mice and rats is driven by changes in trabecular number (which we did not measure here), and that human bone volume fraction variation is driven by changes in trabecular thickness. However, in contrast to our findings, Barak et al. (2013) found no correlation between bone volume fraction and body mass, likely because the correlation was assessed across the full range of body masses in the sample. The relationship between bone volume fraction and mass in our study is stronger than in a number of studies focusing on larger body mass ranges and absolutely larger median body masses (Doube et al., 2011; Barak et al., 2013; Ryan & Shaw, 2013), but it is not clear if the signal we recovered is specifically related to mass range rather than mean. One previous study (Fajardo et al., 2013) noted that there appears to be an asymptote in the relationship between bone volume fraction and mass: in animals larger than about 600–700 g, the relationship flattens to a slope of approximately 0 (Fajardo et al., 2013: fig. 3A). The presence of such an asymptote could explain the stronger body size signal we see in smaller animals, and potentially reveal a fundamental structural limit that elucidates the way that the skeletons of the smallest mammals adapt to habitual stresses. Increased sampling surrounding the possible inflection point will facilitate further exploration of its implications, and could be accomplished using additional rodent species.

ISOMETRIC SCALING IN TRABECULAR THICKNESS

Compared to bone volume fraction, trabecular thickness has a more robust correlation with body mass, scaling isometrically with a high R² (Table 4). Coupled with the small values for trabecular thickness CV (Table 2), this suggests a very close relationship between mass and trabecular thickness. Larger animals have absolutely thicker trabeculae, but relative to body size, their trabeculae are of similar thickness to those of smaller animals (Ulrich et al., 1999). Thicker trabeculae do experience less strain than thinner ones (Doube et al., 2011), which may be related to withstanding higher stresses at larger body masses. We also found that larger animals have absolutely larger trabecular separation, but the relationship is weak and negatively allometric (Table 4). This means that, to a limited degree, larger animals have absolutely larger, but relatively smaller, separation between their trabeculae. Isometry in trabecular thickness and slight negative allometry in trabecular separation make sense in light of the slight positive allometry in bone volume fraction: holding trabecular thickness constant and slightly decreasing the space between trabecular struts will on average result in slightly higher overall density.

In comparing our results to the existing trabecular bone literature, we found only one other study that recovered isometry in trabecular thickness: a study of the lumbar vertebrae in small-to-medium strepsirrhine primates (Fajardo et al., 2013). All the other studies we examined, including those focused on femora (Doube et al., 2011; Ryan & Shaw, 2013; Mielke et al., 2018), femora and tibiae (Aguirre et al., 2020), pelvic bone (Webb, 2021), and foot and ankle elements (Saers et al., 2019) found negative allometry in trabecular thickness. A number of workers have noted that negative allometry in trabecular thickness is necessitated by the physiological limitations of bone, and the sheer range of body size across vertebrates. Doube et al. (2011) in particular made a compelling argument to demonstrate this. They showed mathematically that isometric scaling of shrew-sized trabeculae would result in centimetre-thick trabeculae when scaled to elephant size, which is much too thick to allow for osteocyte nutrient exchange (Lozupone & Favia, 1990). Conversely, if elephant-sized trabeculae were isometrically scaled down to shrew size, shrew trabeculae would be only 3 µm wide—as they note, smaller than a single osteocyte (Doube *et al.*, 2011).

If it is therefore unreasonable to assume that trabecular thickness could have isometric scaling across the full range of mammalian body size in any trabecular tissue, it is unlikely that the anatomical origin of the tissue in our study is the only reason that we recover isometry. It is more likely due to both anatomical origin and body mass range: in smallerbodied mammals, trabecular thickness scales with isometry in vertebrae, but not in femora. For example: Fajardo et al. (2013) included species with masses from 42 to 2440 g in their vertebral study and found isometry in trabecular thickness. Mielke et al. (2018) included masses from a similar range, 16.5 to 3880 g (Jones et al., 2009) in their femoral study, and found negative allometry in trabecular thickness. However, these two studies examined different taxonomic groups [strepsirrhine primates (Fajardo et al., 2013) and sciuromorphs (Mielke et al., 2018)], with distinct locomotor types. A study of strepsirrhine femora (Ryan & Ketcham, 2002) recovered negative allometry in trabecular thickness, but also examined no species smaller than 267 g, making it difficult to compare to the vertebral study. Although at least one study examined trabecular structure of both vertebrae and limb bones (humeri) in each included specimen (Amson & Bibi, 2021), that study did not report trabecular thickness for both. To thoroughly address this question, and to further test hypotheses about the different selective pressures on trabecular bone at small body sizes, work should be conducted examining allometric scaling in trabecular bone of vertebrae and femora sets from every individual, including plenty of animals under 200 g in mass.

INTRASPECIFIC VARIATION

Although studies of trabecular bone morphology often include samples from more than one specimen per species, intraspecific variation is not usually a focus of discussion. Lack of understanding regarding normal intraspecific variation is a problem for workers interested in linking trabecular bone morphology to ecology or function: if we do not have a good sense of how morphology normally varies within a species, how can we determine what amount of variation is unusual or potentially ecomorphologically informative? Furthermore, how do we know how many specimens

to sample to uncover the whole breadth of trabecular bone morphology present in a species?

We sampled a moderate number of individuals per species (N = 6, Table 2), enough to get some sense of intraspecific variation in all 11 taxa. The resulting CVs (Table 2) showed mostly the same patterns as those in other studies with similar or slightly larger sample sizes (Fajardo $et\ al.$, 2007a, N=2-12; Fajardo et al., 2013, N = 2-6). Few studies report CV, even when examining multiple specimens. The small values we report for CV in trabecular thickness suggest that it is relatively consistent within a species, and that it can be determined reasonably well with just a few individuals in our probabilistic, multilevel framework. The values for bone volume fraction and trabecular separation are higher, and indicate that more specimens may be needed to capture the extent of variation in these metrics. However, one additional study of humans and great apes with samples of 12, 14 and 20 specimens (Georgiou et al., 2019) obtained CVs for bone volume fraction and trabecular separation slightly lower than ours (ranging approximately 8-17% for both, their table 2), suggesting that the three-fold increase in the number of specimens we sampled might make little difference.

The primary finding resulting from our intraspecific variation measurements is the enormous specieslevel CVs in connectivity density: up to 77% of the mean in our study (Table 2) and up to 80% in others (Fajardo et al., 2007a). It is possible that small segmentation errors are responsible for part of the high variation in connectivity density: a loss of even a few pixels connecting very faint or thin trabeculae could skew the connectivity measurement. However, based on qualitative inspections of the variation we see in these animals, segmentation error is probably not the only driver. Figure 4, especially the inset slices through vertebrae, emphasizes this pattern, showing high degrees of intraspecific variation along the connectivity density vector, especially for Archboldomys maximus, Apomys sierrae and Chrotomys silaceus. This huge degree of intraspecific variation in connectivity density may have functional or adaptive implications, but they have so far not been discussed. This lack of discussion is likely due to a lack of basic information about the influences on connectivity density: how is function affected when it is high or low? How does development play a role? If we do not understand the developmental drivers and functional correlates of connectivity density, it is much more difficult to test hypotheses about why it varies so much more than other trabecular bone metrics. Unfortunately, relationships between connectivity and mechanical properties are nebulous, and some work indicates that there is no reliable relationship at all between connectivity density and mechanical/elastic

properties of bone (Odgaard & Gundersen, 1993). One study found a weak relationship between increasing connectivity density and decreasing bone stiffness 'if any relationship exists' (Kabel et al., 1999: p.119). If this weak relationship exists, we might expect bone volume fraction, which is correlated with strength and stiffness (Nazarian et al., 2008; Musy et al., 2017), to decrease with increasing connectivity density and decreasing bone stiffness. Yet in the present study, bone volume fraction and connectivity density are not correlated (Pearson coefficient = -0.16, p = 0.18). Previously, bone volume fraction and connectivity density have also been shown to be unrelated or weakly related (Odgaard & Gundersen, 1993; Kabel et al., 1999; Mittra et al., 2005). Because connectivity density appears to have little utility in predicting the mechanical properties of trabecular bone, and little correlation with other trabecular bone metrics (Mittra et al., 2005), it may be capturing a distinct piece of physiological or metabolic life history information (e.g., Ruimerman et al., 2005).

SUBSTRATE USE, INTERTAXON VARIATION AND PHYLOGENETIC SIGNAL

Although body size is one of the primary factors influencing trabecular bone morphology, the differences in how animals use their bodies to interact with their substrate also factors into that morphology (Cotter et al., 2009; Barak et al., 2011; Ryan & Shaw, 2012, 2015; Mielke et al., 2018). The earthworm mice included in this study exhibit a variety of different substrate use strategies, which could be reflected in their trabecular bone morphology. However, they are also an endemic group of terrestrial rodents that have been evolving together in isolation for approximately 8 Myr (Rowsey et al., 2018). This means that they are similar not only because of shared phylogenetic history, but because of shared environmental history. Apart from elevation-related differences in habitat, they have experienced the same environmental stressors (e.g., typhoons) throughout their evolution, and shared their habitats with the same or similar assemblages of other organisms. Some baseline degree of similarity in chrotomyins is probably due to this shared environmental history, but we focus here on the quantifiable effects of shared phylogenetic history, which can be specifically tracked across different morphological traits.

Other trabecular bone studies of several mammalian clades have found varying levels of phylogenetic signal across trabecular bone metrics. This variation could be due to the range of different phylogenetic comparative methods they used, or to stronger or more varied extrinsic selective pressure in particular clades. Mostly these studies have recovered small degrees of

phylogenetic signal in some trabecular bone metrics (Ryan & Shaw, 2013; Amson et al., 2017; Plasse et al., 2019), as measured by Pagel's lambda (Pagel, 1999) or Blomberg's K (Blomberg et al., 2003). Incorporation of phylogenetic covariation in estimates of trabecular bone morphology has a consistent effect in our data: it increases the 89% credible intervals in both genusand species-level analyses, but in most cases does not cause much change in the actual estimate of the mean for each group (Figs 6, 7). The largest changes resulting from incorporation of phylogenetic information occur in the two analyses with the highest mean estimates for lambda: the genus-level analyses of bone volume fraction and trabecular thickness (Fig. 6).

Our data have an extra layer of difficulty for elucidating which similarities and differences are phylogenetic effects, and which are related to function, because our substrate-use categories are strongly correlated with phylogenetic structure (Table 1, Fig. 5). In our sample, several substrate-use transitions occur only once on the phylogeny, representing single replicates of the test of functional linkage between morphology and substrate use type. With only one replicate, it is extremely challenging to confidently link a morphological character to membership in a particular ecological group (Adams & Collyer, 2018; Uyeda et al., 2018). This conflation of phylogenetic and ecological signal has been noted in previous trabecular bone work (Amson et al., 2017; Amson & Kilbourne, 2019; Zack et al., 2022, 2023), and has been shown to reduce the statistical power of phylogenetically informed ANOVAs (Adams & Collyer, 2018). Although we do not have quantitative data on how this phenomenon affects posterior probability distributions in our analyses, it likely adds to the inherent difficulty in separating phylogenetic from functional signal. With this caveat in mind, we address potential functional signals below.

RELATIVE DEGREE OF FOSSORIALITY AND CHROTOMYS

The most generalist genus of earthworm mice is *Apomys* (subgenus *Megapomys*, Heaney *et al.*, 2011), which includes terrestrial quadrupeds between 58 g and 128 g in mass (Heaney *et al.*, 2016a). *Apomys* has relatively unspecialized ambulatory locomotion for a small mammal, and all species forage on the surface of the ground (Heaney *et al.*, 2011, 2016a), such that the variation in mechanical environment among species is probably small. Both *Soricomys* and *Archboldomys* are frequently described as shrew-like animals, and are the smallest animals in our data set (Table 1, Figs 1, 8). They are terrestrial but forage for invertebrates in leaf litter on the surface of the ground. They should not be considered fossorial or semifossorial, but have slightly different substrate use strategies than *Apomys*. In

contrast, the genus *Chrotomys* includes active diggers that should be considered semifossorial. Because the posterior presacral vertebral column (lumbar vertebrae) and the sacrum itself are used to transmit force to the stable pelvic girdle during forelimb digging, the vertebrae of semifossorial animals are subjected to different mechanical environments compared to non-fossorial animals (Hildebrand, 1985; Gaudin & Biewener, 1992; Oliver et al., 2016; Tague, 2020). We therefore expected to find the most closely packed trabecular structure in *Chrotomys*, with higher bone volume fraction and trabecular thickness, which are directly related to a bone's capability to withstand failure (strength; Ulrich et al., 1999; Musy et al., 2017). Instead, Soricomys has the highest estimated mean bone volume fraction and trabecular thickness, whereas Rhynchomys has the lowest. Estimates for Chrotomys, Apomys and Archboldomys fall close to the global mean, both with and without the inclusion of phylogeny in the model. This would seem to suggest essentially no link between semifossorial behaviour and spatially dense trabecular bone. However, when considering species-level differences, the picture becomes more nuanced, particularly with regard to trabecular thickness.

Among the several species of *Chrotomys* there is variation in habitat elevation, which affects the hardness of the substrate in which the animal digs. Higher elevation forested habitats frequented by C. silaceus and C. whiteheadi have a thick (10 cm-1 m) layer of surface humus, which is relatively loose and uncompacted (Heaney et al., 2016a). Chrotomys mindorensis is more common at lower elevations, where the primary available substrate is a more compact, dense soil. Chrotomys mindorensis and C. whiteheadi have the highest and second-highest estimates for trabecular thickness, respectively, with C. silaceus falling much lower, well below the global mean. Individually, larger trabeculae experience less strain and are less likely to crack under load (Doube et al., 2011; Turunen et al., 2020), so the increased trabecular thickness relative to body size in the most fossorial animal in the dataset (*C. mindorensis*) could indeed provide increased resistance to highermagnitude forces. Doube et al. (2011) suggested that the positive correlation between trabecular thickness and body size has to do with maintaining functional homeostasis: a larger animal's trabeculae are under higher load, but their larger size reduces their strain. If C. mindorensis experiences higher habitual loads in its vertebral trabecular bone due to bracing during digging behaviour in dense substrate, then higher trabecular thickness may allow it to maintain similar trabecular strain. However, the fact that the less fossorial C. whiteheadi has the second highest trabecular thickness, and is the sister taxon to C.

2003).

mindorensis, indicates that high trabecular thickness cannot be entirely ascribed to functional demands, and likely has a phylogenetic component.

AN UNEXPECTED CHARACTER SUITE IN RHYNCHOMYS Although its locomotion incorporates bipedal hopping, the hopping gait and associated morphology in Rhynchomys is not as extreme as in fully bipedal heteromyids (e.g., kangaroo rats) and dipodids (e.g., jerboas). Its locomotion is instead characterized by the use of the hindlimbs in a symmetrical but not fully bipedal gait (bounding or half-bounding; L. Heaney, pers. obs.; Hildebrand, 1977). In some mammals, specialized use of the half-bound gait is associated with elongation of the lumbar spine (Jones & German, 2014), which increases efficiency of the gait by allowing greater extension of the body after lift-off (Schilling & Hackert, 2006; Jones & German, 2014). Rhynchomys does not have elongate vertebral centra compared to other earthworm mice (Fig. 8), and it has the same number of lumbar vertebrae as other species in the clade (Supporting Information, Table S1). This suggests that *Rhynchomys* does not have any particular gross anatomical adaptations in the lumbar spine to increase bounding efficiency. However, the lumbar vertebrae of R. labo do stand out from others in the sample in having the lowest bone volume fraction for its body size of any genus or species, driven by a relatively low trabecular thickness and relatively high trabecular separation (Fig. 7). From a material standpoint, these characteristics indicate that the trabecular bone of *Rhynchomys* is weaker and more susceptible to failure under compressive load compared to that of other earthworm mice (Goulet et al., 1994; Ulrich et al., 1999; Hernandez et al., 2001; Bevill & Keaveny, 2009). This is unexpected given the higher bone and muscle strains associated with standing bipedal jumps (Emerson, 1985; Alexander,

There are a number of potential explanations for this unusual suite of characteristics. First, it is possible that the mechanical environment of *Rhynchomys* is not sufficiently different from that of the non-hopping mammals in our study to necessitate trabecular bone adaptation. Even relatively extreme artificial manipulations of environment (e.g., Barak et al., 2011) may only produce slight changes in trabecular bone characteristics, so the minor changes in force regime associated with brief bouts of bipedal hopping may also be insufficient to have a significant effect. Nevertheless, an insufficiently stressful mechanical environment fails to explain why the mean bone volume fraction is markedly below the global mean. Rhynchomys also has slightly higher than average connectivity density. as does the other taxon with the lowest bone volume fraction (*Chrotomys silaceus*). It is possible that there is some functional tradeoff or compensation occurring here: an increase in trabecular connections to compensate for lower strength or stiffness associated with lower bone volume fraction. As noted above, however, the mechanical significance of connectivity is unclear, and requires additional study.

CONCLUSION

This work uses a monophyletic radiation of murines (Chrotomyini) to examine the various influences on trabecular bone morphology in small mammals. We found a strong relationship between trabecular bone morphology and body mass, with an especially close linkage between mass and trabecular thickness. The allometric scaling patterns we observe suggest that trabecular bone shape scales differently in small mammals compared to larger mammals. In our data set of mammals with body masses of 225 g or under, bone volume fraction and trabecular thickness increase more quickly with increasing body size than they do in larger mammals. In chrotomyins, trabecular thickness and bone volume fraction are also linked to phylogenetic structure, whereas trabecular spacing and connectivity density show a weaker relationship with phylogeny. Substrate-use groupings in this clade are also closely associated with phylogenetic structure, making it difficult to support links between specific substrate-use types and trabecular morphology. Some correlation among phylogeny, morphology and substrate use is not unexpected, as a result of the shared evolutionary history and sympatric occurrence of the members of this endemic clade.

Unusual suites of trabecular bone qualities characterize the two most functionally distinct species in our sample (R. labo and C. mindorensis), but some aspects of their morphology (e.g., connectivity density) cannot be confidently attributed to function based on the current literature. Future work should examine how body size relates to selective pressures on the skeletons of small-bodied mammals, and link trabecular bone scaling to gross vertebral morphology and cortical thickness to gain a more holistic perspective on body size and vertebral function. Studies should also consider functional performance in vertebral trabecular bone, and the similarities or differences in functional signal across trabecular bone from different anatomical sites. It is apparent from this and other recent studies that the variation in trabecular bone morphology across mammals is great. Continued study of its relationship with body size, phylogeny and function will enable workers to use it as a more effective tool in understanding how

mammalian skeletons model and adapt to deal with everyday forces.

ACKNOWLEDGEMENTS

Many thanks to Danilo Balete, Eric Rickart and the broader Philippine Mammal Project team (https:// www.philippinemammalproject.com/), who collected the specimens used in this work; to the Philippine Department of Environment and Natural Resources, for issuing research and collecting permits to L.R.H.; to the Field Museum of Natural History Mammalogy staff (Adam Ferguson, Lauren Johnson, Lauren Nassef, Bruce Patterson and John Phelps). who provided access to specimens and assistance with specimen loans; to April Neander and Zhe-Xi Luo, who provided access to the University of Chicago PaleoCT scanning facility; to the Field Museum Women's Board and Bass Family, who provided funding to S.M.S; to the Angielczyk group for useful discussions regarding this work; and to two anonymous reviewers for their highly constructive and thoughtful comments that greatly improved the manuscript. We have no conflicts of interest to declare.

DATA AVAILABILITY

The data underlying this article are available in the article and in its online supplementary materials, and in the Dryad Digital Repository (Smith *et al.*, 2023).

REFERENCES

- Adams DC, Collyer ML. 2018. Phylogenetic ANOVA: groupclade aggregation, biological challenges, and a refined permutation procedure. *Evolution* 72: 1204–1215.
- Aguirre TG, Ingrole A, Fuller L, Seek TW, Fiorillo AR, Sertich JJW, Donahue SW. 2020. Differing trabecular bone architecture in dinosaurs and mammals contribute to stiffness and limits on bone strain. *PLoS ONE* 15: e02370421–20.
- **Alexander RM. 2003**. *Principles of animal locomotion*. Princeton: Princeton University Press.
- **Álvarez A, Ercoli MD, Prevosti FJ. 2013**. Locomotion in some small to medium-sized mammals: a geometric morphometric analysis of the penultimate lumbar vertebra, pelvis and hindlimbs. *Zoology* **116**: 356–371.
- Amson E, Arnold P, van Heteren AH, Canoville A, Nyakatura JA. 2017. Trabecular architecture in the forelimb epiphyses of extant xenarthrans (Mammalia). Frontiers in Zoology 14: 1-17.
- Amson E, Bibi F. 2021. Differing effects of size and lifestyle on bone structure in mammals. *BMC Biology* 19: 1–18.

- Amson E, Kilbourne BM. 2019. Trabecular bone architecture in the stylopod epiphyses of mustelids (Mammalia, Carnivora). Royal Society Open Science 6: 190938
- Balete DS, Rickart EA, Rosell-Ambal RGB, Jansa S, Heaney LR. 2007. Descriptions of two new species of *Rhynchomys* Thomas (Rodentia: Muridae: Murinae) from Luzon Island, Philippines. *Journal of Mammalogy* 88: 287–301.
- Balete DS, Rickart EA, Heaney LR, Alviola PA, Duya MV, Duya MRM, Sosa T, Jansa SA. 2012. Archboldomys (Muridae: Murinae) reconsidered: a new genus and three new species of shrew mice from Luzon Island, Philippines. American Museum Novitates 3754: 1–60.
- Balete DS, Rickart EA, Heaney LR. 2006. A new species of the shrew-mouse, *Archboldomys* (Rodentia: Muridae: Murinae), from the Philippines. *Systematics and Biodiversity* 4: 489–501.
- Barak MM, Lieberman DE, Hublin JJ. 2011. A Wolff in sheep's clothing: trabecular bone adaptation in response to changes in joint loading orientation. *Bone* 49: 1141–1151.
- Barak MM, Lieberman DE, Hublin JJ. 2013. Of mice, rats and men: trabecular bone architecture in mammals scales to body mass with negative allometry. *Journal of Structural Biology* 183: 123–131.
- Bevill G, Keaveny TM. 2009. Trabecular bone strength predictions using finite element analysis of micro-scale images at limited spatial resolution. *Bone* 44: 579–584.
- **Biewener AA. 1989.** Scaling body support in mammals: limb posture and muscle mechanics. *Science* **245**: 45–48.
- **Biewener AA. 1990**. Biomechanics of mammalian terrestrial locomotion. *Science* **250**: 1097–1103.
- **Blomberg SP**, **Garland T**, **Ives AR. 2003**. Testing for phylogenetic signal in comparative data: behavioral traits are more labile. *Evolution* **57**: 717–745.
- Boszczyk BM, Boszczyk AA, Putz R. 2001. Comparative and functional anatomy of the mammalian lumbar spine. Anatomical Record 264: 157–168.
- Bouckaert RR, Heled J, Kühnert D, Vaughan TG, Wu CH, Xie D, Suchard MA, Rambaut A, Drummond AJ. 2014.
 BEAST 2: a software platform for Bayesian evolutionary analysis. PLoS Computational Biology 10: e10035371–7.
- Bouckaert RR, Vaughan TG, Barido-Sottani J, Duchêne S, Fourment M, Gavryushkina A, Heled J, Jones G, Kühnert D, de Maio N, Matschiner M, Mendes FK, Müller NF, Ogilvie HA, du Plessis L, Popinga A, Rambaut A, Rasmussen D, Siveroni I, Suchard MA, Wu CH, Xie D, Zhang C, Stadler T, Drummond AJ. 2019. BEAST 2.5: an advanced software platform for Bayesian evolutionary analysis. PLoS Computational Biology 15: 1–28.
- Briggs DEG. 2017. Seilacher, Konstruktions-Morphologie, Morphodynamics, and the evolution of form. *Journal of Experimental Zoology Part B: Molecular and Developmental Evolution* 328: 197–206.
- **Bürkner PC. 2017**. brms: an R package for Bayesian multilevel models using Stan. *Journal of Statistical Software* **80**: 1–28.
- **Bürkner PC. 2018**. Advanced Bayesian multilevel modeling with the R package brms. *The R Journal* **10**: 395.

- Bürkner PC. 2021. Bayesian item response modeling in R with brms and Stan. Journal of Statistical Software 100:
- Carpenter B, Gelman A, Hoffman MD, Lee D, Goodrich B, Betancourt M, Brubaker M, Guo J, Li P, Riddell A. 2017. Stan: a probabilistic programming language. Journal of Statistical Software 76: 1–32.
- Chen X, Milne N, O'Higgins P. 2005. Morphological variation of the thoracolumbar vertebrae in Macropodidae and its functional relevance. Journal of Morphology 266: 167-181.
- Christen P, Ito K, van Rietbergen B. 2015. A potential mechanism for allometric trabecular bone scaling in terrestrial mammals. Journal of Anatomy 226: 236-243.
- Christiansen P. 1999. Scaling of mammalian long bones: small and large mammals compared. Journal of Zoology 247: 333-348.
- Cotter MM, Simpson SW, Latimer BM, Hernandez CJ. 2009. Trabecular microarchitecture of hominoid thoracic vertebrae. Anatomical Record 292: 1098-1106.
- Cowin SC. 1986. Wolff's law of trabecular architecture at remodeling equilibrium. Journal of Biomechanical Engineering 108: 83-88.
- Currey JD. 2003. The many adaptations of bone. Journal of Biomechanics 36: 1487-1495.
- Domander R, Felder AA, Doube M. 2021. BoneJ2 refactoring established research software. Wellcome Open Research 6: 37.
- Doube M. Kłosowski MM. Wiktorowicz-Conrov AM. Hutchinson JR, Shefelbine SJ. 2011. Trabecular bone scales allometrically in mammals and birds. Proceedings of the Royal Society B: Biological Sciences 278: 3067-3073.
- Doube M, Rimadoma, Rueden C, Felder AA, Hiner M, Eglinger J. 2021. bonej-org/BoneJ2: styloid-r11 (bonej-7.0.11). Zenodo. https://doi.org/10.5281/zenodo.4635373.
- Dunmore CJ, Kivell TL, Bardo A, Skinner MM. 2019. Metacarpal trabecular bone varies with distinct handpositions used in hominid locomotion. Journal of Anatomy **235**: 45-66.
- Emerson S. 1985. Jumping and leaping. In: Hildebrand M, Bramble DM, Liem KF, Wake DB, eds. Functional vertebrate morphology. Cambridge: Belknap Press of Harvard University, 58-72.
- English AW. 1980. The functions of the lumbar spine during stepping in the cat. Journal of Morphology 165: 55–66.
- Fajardo RJ, Desilva JM, Manoharan RK, Schmitz JE, Maclatchy LM, Bouxsein ML. 2013. Lumbar vertebral body bone microstructural scaling in small to medium-sized strepsirhines. Anatomical Record 296: 210-226.
- Fajardo RJ, Hernandez E, O'Connor PM. 2007b. Postcranial skeletal pneumaticity: a case study in the use of quantitative microCT to assess vertebral structure in birds. Journal of Anatomy 211: 138-147.
- Fajardo RJ, Müller R, Ketcham RA, Colbert M. 2007a. Nonhuman anthropoid primate femoral neck trabecular architecture and its relationship to locomotor mode. Anatomical Record 290: 422-436.
- Fernando ES, Suh MH, Lee J, Lee DK. 2008. Forest formations of the Philippines. Seoul: GeoBook.

- Gaudin TJ, Biewener AA. 1992. The functional morphology of xenarthrous vertebrae in the armadillo Dasypus novemcinctus (Mammalia, Xenarthra). Journal of Morphology 214: 63-81.
- Georgiou L, Kivell TL, Pahr DH, Buck LT, Skinner MM. 2019. Trabecular architecture of the great ape and human femoral head. Journal of Anatomy 234: 679–693.
- Gorissen BMC, Wolschrijn CF, van Vilsteren AAM, van Rietbergen B, van Weeren PR. 2016. Trabecular bone of precocials at birth; are they prepared to run for the wolf(f)? Journal of Morphology 277: 948-956.
- Goulet RW, Goldstein SA, Ciarelli MJ, Kuhn JL, Brown MB, Feldkamp LA. 1994. The relationship between the structural and orthogonal compressive properties of trabecular bone. Journal of Biomechanics 27: 375-389.
- Granatosky MC, Miller CE, Boyer DM, Schmitt D. 2014. Lumbar vertebral morphology of flying, gliding, and suspensory mammals: implications for the locomotor behavior of the subfossil lemurs Palaeopropithecus and Babakotia. Journal of Human Evolution 75: 40-52.
- Gu X, Fu YX, Li WH. 1995. Maximum likelihood estimation of the heterogeneity of substitution rate among nucleotide sites. Molecular Biology and Evolution 12: 546-557.
- Hadfield JD, Nakagawa S. 2010. General quantitative genetic methods for comparative biology: phylogenies, taxonomies and multi-trait models for continuous and categorical characters. Journal of Evolutionary Biology 23: 494-508.
- Heaney LR, Balete DS, Dolar ML, Alcala AC, Dans ATL, Gonzales PC, Ingle NR, Lepiten MV, Oliver WLR, Ong PS, Rickart EA, Tabaranza BR Jr, Utzurrum RCB. 1998. A synopsis of the mammalian fauna of the Philippine Islands. Fieldiana Zoology, new series 88: 1-61.
- Heaney LR, Balete DS, Duya MRM, Duya MV, Jansa SA, Steppan SJ, Rickart EA. 2016b. Doubling diversity: a cautionary tale of previously unsuspected mammalian diversity on a tropical oceanic island. Frontiers of Biogeography 8: 1-19.
- Heaney LR, Balete DS, Rickart EA, Alviola PA, Duya MRM, Duya MV, Veluz MJ, VandeVrede L, Steppan SJ. 2011. Chapter 1: Seven new species and a new subgenus of forest mice (Rodentia: Muridae: Apomys) from Luzon Island. Fieldiana Life and Earth Sciences 2: 1-60.
- Heaney LR, Balete DS, Rickart EA, Niedzielski A. 2016a. The mammals of Luzon Island: biogeography and natural history of a Philippine fauna. Baltimore: JHU Press.
- Hernandez CJ, Beaupré GS, Keller TS, Carter DR. 2001. The influence of bone volume fraction and ash fraction on bone strength and modulus. Bone 29: 74-78.
- Hildebrand M. 1959. Motions of the running cheetah and horse. Journal of Mammalogy 40: 481.
- Hildebrand M. 1977. Analysis of asymmetrical gaits. Journal of Mammalogy 58: 131-156.
- **Hildebrand M. 1985**. Digging of quadrupeds. *Functional* Vertebrate Morphology 6: 89–109.
- Huiskes R, Rulmerman R, van Lenthe GH, Janssen JD. 2000. Effects of mechanical forces on maintenance and adaptation of form in trabecular bone. Nature 405: 704-706.

- Jansa SA, Barker FK, Heaney LR. 2006. The pattern and timing of diversification of Philippine endemic rodents: evidence from mitochondrial and nuclear gene sequences. Systematic Biology 55: 73–88.
- Jones KE, Bielby J, Cardillo M, Fritz SA, O'Dell J, Orme CDL, Safi K, Sechrest W, Boakes EH, Carbone C, Connolly C, Cutts MJ, Foster JK, Grenyer R, Habib M, Plaster CA, Price SA, Rigby EA, Rist J, Teacher A, Bininda-Emonds ORP, Gittleman JL, Mace GM, Purvis A. 2009. PanTHERIA: a species-level database of life history, ecology, and geography of extant and recently extinct mammals. *Ecology* 90: 2648.
- Jones KE. 2015a. Evolutionary allometry of lumbar shape in Felidae and Bovidae. Biological Journal of the Linnean Society 116: 721–740.
- Jones KE. 2015b. Evolutionary allometry of the thoracolumbar centra in felids and bovids. *Journal of Morphology* 276: 818–831.
- Jones KE, Angielczyk KD, Polly PD, Head JJ, Fernandez V, Lungmus JK, Tulga S, Pierce SE. 2018. Fossils reveal the complex evolutionary history of the mammalian regionalized spine. Science 361: 1249–1252.
- Jones KE, German RZ. 2014. Ontogenetic allometry in the thoracolumbar spine of mammal species with differing gait use. Evolution & Development 16: 110–120.
- Justiniano R, Schenk JJ, Balete DS, Rickart EA, Esselstyn JA, Heaney LR, Steppan SJ. 2015. Testing diversification models of endemic Philippine forest mice (*Apomys*) with nuclear phylogenies across elevational gradients reveals repeated colonization of isolated mountain ranges. *Journal of Biogeography* 42: 51–64.
- Kabel J, Odgaard A, van Rietbergen B, Huiskes R. 1999.Connectivity and the elastic properties of cancellous bone.Bone 24: 115–120.
- Keaveny TM, Hayes WC. 1993. A 20-year perspective on the mechanical properties of trabecular bone. *Journal of Biomechanical Engineering* 115: 534–542.
- Kimura Y, Hawkins MTR, McDonough MM, Jacobs LL, Flynn LJ. 2015. Corrected placement of *Mus-Rattus* fossil calibration forces precision in the molecular tree of rodents. *Scientific Reports* 5: 1–9.
- **Kivell TL. 2016**. A review of trabecular bone functional adaptation: what have we learned from trabecular analyses in extant hominoids and what can we apply to fossils? *Journal of Anatomy* **228**: 569–594.
- Kothari M, Keaveny TM, Lin JC, Newitt DC, Majumdar S. 1999. Measurement of intraspecimen variations in vertebral cancellous bone architecture. *Bone* 25: 245–250.
- Lanfear R, Calcott B, Ho SYW, Guindon S. 2012.
 PartitionFinder: combined selection of partitioning schemes and substitution models for phylogenetic analyses. *Molecular Biology and Evolution* 29: 1695–1701.
- Lanyon LE, Goodship AE, Pye CJ, MacFie JH. 1982.
 Mechanically adaptive bone remodelling. Journal of Biomechanics 15: 141-154.
- Lozupone E, Favia A. 1990. The structure of the trabeculae of cancellous bone. 2. Long bones and mastoid. Calcified Tissue International 46: 367–372.

- Main RP, Shefelbine SJ, Meakin LB, Silva MJ, Meulen MCH, Willie BM. 2020. Murine axial compression tibial loading model to study bone mechanobiology: implementing the model and reporting results. *Journal of Orthopaedic Research* 38: 233–252.
- Main RP, Lynch ME, van der Meulen MCH. 2014. Loadinduced changes in bone stiffness and cancellous and cortical bone mass following tibial compression diminish with age in female mice. *Journal of Experimental Biology* 217: 1775–1783.
- McElreath R. 2020. Statistical rethinking. New York: Chapman and Hall/CRC.
- Mielke M, Wölfer J, Arnold P, van Heteren AH, Amson E, Nyakatura JA. 2018. Trabecular architecture in the sciuromorph femoral head: allometry and functional adaptation. *Zoological Letters* 4: 1–11.
- Miller MA, Pfeiffer W, Schwartz T. 2010. Creating the CIPRES Science Gateway for inference of large phylogenetic trees. 2010 Gateway Computing Environments Workshop, GCE 2010: 1–8.
- Mittra E, Rubin C, Qin YX. 2005. Interrelationship of trabecular mechanical and microstructural properties in sheep trabecular bone. *Journal of Biomechanics* 38: 1229–1237.
- Musser GG, Freeman PW. 1981. A new species of Rhynchomys (Muridae) from the Philippines. Journal of Mammalogy 62: 154–159
- Musser GG, Gordon LK, Sommer H. 1982. Species-limits in the Philippine murid, *Chrotomys. Journal of Mammalogy* **63**: 514–521.
- Musy SN, Maquer G, Panyasantisuk J, Wandel J, Zysset PK. 2017. Not only stiffness, but also yield strength of the trabecular structure determined by non-linear μFE is best predicted by bone volume fraction and fabric tensor. *Journal of the Mechanical Behavior of Biomedical Materials* 65: 808–813.
- Nazarian A, von Stechow D, Zurakowski D, Müller R, Snyder BD. 2008. Bone volume fraction explains the variation in strength and stiffness of cancellous bone affected by metastatic cancer and osteoporosis. *Calcified Tissue International* 83: 368–379.
- Odgaard A, Gundersen HJG. 1993. Quantification of connectivity with special emphasis on 3D reconstructions. *Bone* 14: 173–182.
- Oliver JD, Jones KE, Hautier L, Loughry WJ, Pierce SE. 2016. Vertebral bending mechanics and xenarthrous morphology in the nine-banded armadillo (*Dasypus novemcinctus*). Journal of Experimental Biology 219: 2991–3002.
- Pagel M. 1999. Inferring the historical patterns of biological evolution. *Nature* 401: 877–884.
- Petrosky AL, Rowsey DM, Heaney LR. 2021. Molecular assessment of dietary niche partitioning in an endemic island radiation of tropical mammals. *Molecular Ecology* 30: 5858–5873.
- Plasse M, Amson E, Bardin J, Grimal Q, Germain D. 2019. Trabecular architecture in the humeral metaphyses of non-avian reptiles (Crocodylia, Squamata and Testudines): lifestyle, allometry and phylogeny. *Journal of Morphology* 280: 982–998.

- Poulet B, de Souza R, Kent AV, Saxon L, Barker O, Wilson A, Chang YM, Cake M, Pitsillides AA. 2015. Intermittent applied mechanical loading induces subchondral bone thickening that may be intensified locally by contiguous articular cartilage lesions. Osteoarthritis and Cartilage 23: 940-8.
- R Core Team. 2022. R: a language and environment for statistical computing. Austria: R Foundation for Statistical Computing.
- Rickart EA, Heaney LR, Goodman SM, Jansa S. 2005. Review of the Philippine genera Chrotomys and Celaenomys (Murinae) and description of a new species. Journal of Mammalogy 86: 415-428.
- Rickart EA, Balete DS, Timm RM, Alviola PA, Esselstyn JA, Heaney LR. 2019. Two new species of shrew-rats (Rhynchomys: Muridae: Rodentia) from Luzon Island, Philippines. Journal of Mammalogy 100: 1112-1129.
- Rolvien T, Hahn M, Siebert U, Püschel K, Wilke HJ, Busse B, Amling M, Oheim R. 2017. Vertebral bone microarchitecture and osteocyte characteristics of three toothed whale species with varying diving behaviour. Scientific Reports 7: 1-10.
- Rowe KC, Achmadi AS, Fabre P, Schenk JJ, Steppan SJ. Esselstyn JA. 2019. Oceanic islands of Wallacea as a source for dispersal and diversification of murine rodents. Journal of Biogeography 46: 2752-2768.
- Rowsey DM, Duya MRM, Ibañez JC, Jansa SA, Rickart EA, Heaney LR. 2022. A new genus and species of shrewlike mouse (Rodentia: Muridae) from a new center of endemism in eastern Mindanao, Philippines. Journal of Mammalogy 103: 1259-1277.
- Rowsey DM, Heaney LR, Jansa SA. 2018. Diversification rates of the 'Old Endemic' murine rodents of Luzon Island, Philippines are inconsistent with incumbency effects and ecological opportunity. Evolution 72: 1420-1435.
- Rowsey DM, Heaney LR, Jansa SA. 2019. Tempo and mode of mandibular shape and size evolution reveal mixed support for incumbency effects in two clades of island-endemic rodents (Muridae: Murinae). Evolution 73: 1411-1427.
- Rowsey DM, Keenan RM, Jansa SA. 2020. Dietary morphology of two island-endemic murid rodent clades is consistent with persistent, incumbent-imposed competitive interactions. Proceedings of the Royal Society B 287: 20192746.
- Ruff C, Holt B, Trinkaus E. 2006. Who's afraid of the big bad Wolff?: 'Wolff's law' and bone functional adaptation. American Journal of Physical Anthropology 129: 484-498.
- Ruimerman R, Hilbers P, van Rietbergen B, Huiskes R. 2005. A theoretical framework for strain-related trabecular bone maintenance and adaptation. Journal of Biomechanics **38**: 931-941.
- Ryan TM, Ketcham RA. 2002. The three-dimensional structure of trabecular bone in the femoral head of strepsirrhine primates. Journal of Human Evolution 43:
- Ryan TM, Krovitz GE. 2006. Trabecular bone ontogeny in the human proximal femur. Journal of Human Evolution 51: 591-602.

- Ryan TM, Shaw CN. 2012. Unique suites of trabecular bone features characterize locomotor behavior in human and nonhuman anthropoid primates. PLoS ONE 7: e41037
- Ryan TM, Shaw CN. 2013. Trabecular bone microstructure scales allometrically in the primate humerus and femur. Proceedings of the Royal Society B: Biological Sciences 280: 20130172
- Ryan TM, Shaw CN. 2015. Gracility of the modern Homo sapiens skeleton is the result of decreased biomechanical loading. Proceedings of the National Academy of Sciences of the United States of America 112: 372-377.
- Saers JPP, Ryan TM, Stock JT. 2019. Trabecular bone structure scales allometrically in the foot of four human groups. Journal of Human Evolution 135: 102654.
- Schilling N, Hackert R. 2006. Sagittal spine movements of small therian mammals during asymmetrical gaits. Journal of Experimental Biology 209: 3925-3939.
- Schindelin J, Arganda-Carreras I, Frise E, Kaynig V, Longair M, Pietzsch T, Preibisch S, Rueden C, Saalfeld S, Schmid B, Tinevez JY, White DJ, Hartenstein V, Eliceiri K, Tomancak P, Cardona A. 2012. Fiji: an open-source platform for biological-image analysis. Nature Methods 9: 676-682.
- **Schwarz G. 1978**. Estimating the dimension of a model. *The* Annals of Statistics 6: 461-464.
- Seilacher A. 1970. Arbeitskonzept Zur Konstruktionsmorphologie. Lethaia 3: 393-396.
- Slijper E. 1946. Comparative biologic anatomical investigations on the vertebral column and spinal musculature of mammals. Verhandelingen der Koninklijke Akademie van Wetenschappen te Amsterdam. Tweede Sectie **17**: 1–128.
- Smit TH, Odgaard A, Schneider E. 1997. Structure and function of vertebral trabecular bone. Spine 22: 2823–2833.
- Smith SM, Angielczyk KD. 2020. Deciphering an extreme morphology: bone microarchitecture of the hero shrew backbone (Soricidae: Scutisorex). Proceedings of the Royal Society B: Biological Sciences 287: 20200457.
- Smith SM, Angielczyk KD. 2022. A shrewd inspection of vertebral regionalization in large shrews (Soricidae: Crocidurinae). Integrative Organismal Biology 4: 1-17.
- Smith SM, Rowsey DM, Nations JA, Angielczyk KD, Heaney LR. 2023. The roles of phylogeny, body size, and substrate use in trabecular bone variation among Philippine earthworm mice (Rodentia: Chrotomyini). Dryad, Dataset. https://doi.org/10.5061/dryad.k3j9kd5c7
- Sode M, Burghardt AJ, Nissenson RA, Majumdar S. 2008. Resolution dependence of the non-metric trabecular structure indices. Bone 42: 728-736.
- Soret M, Bacharach SL, Buvat I. 2007. Partial-volume effect in PET tumor imaging. Journal of Nuclear Medicine **48**: 932-945.
- Swartz SM, Parker A, Huo C. 1998. Theoretical and empirical scaling patterns and topological homology in bone trabeculae. Journal of Experimental Biology 201: 573-590.
- Tague RG. 2020. Commonality in pelvic anatomy among three fossorial, scratch-digging, mammalian species. Journal of Mammalian Evolution 27: 315-327.

- Tamura K, Nei M. 1993. Estimation of the number of nucleotide substitutions in the control region of mitochondrial DNA in humans and chimpanzees. *Molecular Biology and Evolution* 10: 512–526.
- Tanck E, Homminga J, van Lenthe GH, Huiskes R. 2001.
 Increase in bone volume fraction precedes architectural adaptation in growing bone. *Bone* 28: 650–654.
- Turunen MJ, le Cann S, Tudisco E, Lovric G, Patera A, Hall SA, Isaksson H. 2020. Sub-trabecular strain evolution in human trabecular bone. *Scientific Reports* 10: 13788
- Ulrich D, van Rietbergen B, Laib A, Ruegsegger P. 1999. The ability of three-dimensional structural indices to reflect mechanical aspects of trabecular bone. *Bone* 25: 55–60.
- Uyeda JC, Zenil-Ferguson R, Pennell MW. 2018. Rethinking phylogenetic comparative methods. Systematic Biology 67: 1091–1109.
- Villemereuil P, Nakagawa S. 2014. General quantitative genetic methods for comparative biology. In: László Zsolt Garamszegi (ed.), Modern phylogenetic comparative methods

- and their application in evolutionary biology. Heidelberg: Springer Berlin, 287–303.
- **Webb NM. 2021.** The functional and allometric implications of hipbone trabecular microarchitecture in a sample of eutherian and metatherian mammals. *Evolutionary Biology* **48**: 346–365.
- Wolff J. 1893. Das gesetz der transformation der knochen. Deutsche Medizinische Wochenschrift 19: 1222–1224.
- Wysocki AM, Tseng JZ. 2018. Allometry predicts trabecular bone structural properties in the carnivoran jaw joint. PLoS ONE 13: 1–15.
- Yule GU. 1924. A mathematical theory of evolution, based on the conclusions of Dr. J. C. Willis, F.R.S. Philosophical Transactions of the Royal Society of London Series B 213: 21–87
- **Zack EH**, **Smith SM**, **Angielczyk KD**. **2022**. Effect of captivity on the vertebral bone microstructure of xenarthran mammals. *Anatomical Record* **305**: 1611–1628.
- **Zack EH**, **Smith SM**, **Angielczyk KD**. 2023. From fairies to giants: untangling the effect of body size, phylogeny, and ecology on vertebral bone microstructure of xenarthran mammals. *Integrative Organismal Biology* **5**: 1–22.

SUPPORTING INFORMATION

Additional supporting information may be found in the online version of this article on the publisher's website:

- Figure S1. Detailed visualization of calculations for trabecular thickness and trabecular separation.
- Figure S2. Pruned maximum clade credibility tree of Chrotomyini inferred using BEAST. Dots at nodes represent relationships inferred with strong support (posterior probability ≥ 0.95). Bars at nodes represent 95% highest posterior density interval of divergence date inferred from the posterior distribution of 4500 trees.
- Table S1. Specimen data and trabecular bone metrics for all specimens included in the present study.
- Table S2. Scan resolution and relative resolution for all specimens included in the present study.
- Table S3. GenBank reference numbers for specimens included in phylogenetic analysis.
- Table S4. Best-fit nucleotide substitution partitioning scheme for phylogenetic analyses.
- Table S5. Full output from genus-level Bayesian multilevel models, with and without inclusion of phylogenetic structure as a group-level effect.
- Table S6. Full output from species-level Bayesian multilevel models, with and without inclusion of phylogenetic structure as a group-level effect.